An integrated chemostratigraphic ($\delta^{13}C$-$\delta^{18}O$-$^{87}Sr/^{86}Sr$-$\delta^{15}N$) study of the Doushantuo Formation in western Hubei Province, South China.

Zhongwu Lan [a,b*], Yuji Sano [b], Takuya Yahagi [b], Kentaro Tanaka [b], Kotaro Shirai [b], Dominic Papineau [c,d], Yusuke Sawaki [e], Takeshi Ohno [f], Mariko Abe [g], Hongwei Yang [h], Hai Liu [h], Tao Jiang [h], Teng Wang [h]

[a] *State Key Laboratory of Lithospheric Evolution, Institute of Geology and Geophysics, Chinese Academy of Sciences, Beijing 100029, China*
[b] *Atmosphere and Ocean Research Institute, The University of Tokyo, Chiba 277-8564, Japan*
[c] *London Centre for Nanotechnology, University College London, London WC1E 6BT, UK*
[d] *Department of Earth Sciences, and Center for Planetary Sciences, University College London, London WC1E 6BT, UK*
[e] *Department of Earth Science and Astronomy, The University of Tokyo, 3-8-1, Komaba, Meguro-ku, Tokyo 153-8902, Japan*
[f] *Department of Chemistry, Faculty of Science, Gakushuin University, Mejiro, 1-5-1, Toshima-ku, Tokyo 171-8588, Japan*
[g] *Department of Subsurface Geobiological Analysis and Research (D-SUGAR), Japan Agency for Marine-Earth Science and Technology (JAMSTEC), 2-15, Natsushima-cho, Yokosuka, Kanagawa 237-0061, Japan*
[h] *Central South Institute of Metallurgical Geology, Yichang 443003, China*

ABSTRACT

High-resolution isotopic analyses were conducted on core samples from the Ediacaran Doushantuo Formation at the Wangjiapeng section, western Hubei Province in South China, whereby two laterally traceable, negative $\delta^{13}C_{carb}$ excursions (EN1 and EN3) were recognized. The magnitude and duration of these excursions permit intra-basinal and inter-basinal correlation, which indicates that they probably represent a global change in seawater composition. The occurrence of decoupled $\delta^{13}C_{car}$-$\delta^{13}C_{org}$ with almost invariable $\delta^{13}C_{org}$ values at Wangjiapeng, Zhongling, Yangjiaping sections is consistent with remineralization of a dissolved organic carbon (DOC) pool by means of sulfate reduction, as recorded in EN3. The synchronous presence of EN3, a shift to higher $^{87}Sr/^{86}Sr$ and decrease of Mn and Fe contents and $\delta^{15}N$ values together points to a glacial influence whereby oxygenation and remineralization of reduced carbon produced ^{13}C-depleted DIC. Glaciations cause a decrease in sea level, which itself leads to increased continental shelf area to be exposed to surface weathering, and ultimately to enhanced delivery of radiogenic ^{87}Sr. The increase of $^{87}Sr/^{86}Sr$ ratios, sulfate and phosphate are consequences of surface runoff into oceanic environments and such perturbations induce biogeochemical changes.

KEY WORDS: Ediacaran chemostratigraphy; $\delta^{13}C$-$\delta^{18}O$-$^{87}Sr/^{86}Sr$-$\delta^{15}N$; Doushantuo Formation; South China; Ediacaran glaciation; open marine environment

1. Introduction

The Ediacaran Period (c. 635-c. 541 Ma) has increasingly attracted worldwide attention because it was during this time interval that glaciations occurred (Pu et al., 2016) and that new animal forms (e.g. bilaterians) and behaviors (e.g. biomineralization and bioturbation) first emerged (McCall, 2006; Xiao et al., 1998, 2014; Muscente et al., 2015). This period witnessed intriguing and unprecedented chemo-oceanographic fluctuations related to a significant oxygenation event and widespread biogeochemical perturbations (Shields-Zhou and Och, 2011). The carbon isotopic record of ancient seawater recorded in marine carbonates serves as a key proxy for exploring these variations, especially the temporal and causal relationships with biological and environmental factors, although they are often ambiguous partly because of the lack of high resolution chemostratigraphic data.

Information on these biological and environmental events is well preserved in the lower-middle Ediacaran Doushantuo Formation in South China (Xiao et al., 2007; Li et al., 2010; Lu et al., 2013; Liu et al., 2014; Cui et al., 2015, 2016; Muscente et al., 2015; Xiao et al., 2016). The Doushantuo Formation is dominated by carbonate, phosphorite, and black shale that show depositional facies varying from shallow-marine shelf to deep-marine basin (Zhu et al., 2007). As such, the Doushantuo Formation presents a natural sedimentological laboratory for chemostratigraphic study. Three striking fluctuations in ocean composition occurred during the deposition of the Doushantuo Formation as evidenced by three negative $\delta^{13}C_{carb}$ excursions, which may record global-scale events following the late Cryogenian glaciation (Jiang et al., 2003; Wang et al., 2008; Tahata et al., 2013; Lu et al., 2013; Zhu et al., 2013; Furuyama et al., 2016; Zhou et al., 2016). These are 1) the negative $\delta^{13}C_{carb}$ excursion (EN1) in the basal Ediacaran cap carbonates that locally exhibits $\delta^{13}C_{carb}$ values down to −48‰ indicative of methane release from a gas hydrate destabilization event (Jiang et al., 2003; Wang et al., 2008), 2) the relatively less negative $\delta^{13}C$ excursion of ca. −5‰ (EN2) in middle Ediacaran strata (Zhou and Xiao, 2007), and 3) the remarkable negative $\delta^{13}C_{carb}$ excursion (EN3) with values as low as −12‰ recorded globally in middle Ediacaran strata (McFadden et al., 2008). These three negative $\delta^{13}C_{carb}$ excursions have been frequently used for correlation of Ediacaran stratigraphy as well as reconstruction of Ediacaran palaeoenvironments in view of their different amplitudes and stratigraphic levels (Zhou and Xiao, 2007; Zhu et al., 2007). However, the origin of these negative $\delta^{13}C_{carb}$ excursions, particularly EN2 and EN3, and their possible global correlation remain unclear, with various models proposed such as involvement of a DOC reservoir or recycled/detrital organic carbon (McFadden et al., 2008; Jiang et al., 2010, 2012; Johnston et al., 2012; Ishikawa et al., 2013; Wang et al., 2016). In view of the potential diagenetic overprinting and variations in the depth of chemocline between different sections, more detailed work is required to give further constraints.

Carbon isotope stratigraphy combined with strontium and nitrogen isotopic stratigraphy, sequence stratigraphy and redox sensitive elements such as Fe and Mn has helped to clarify some problematic correlations of Ediacaran sedimentary successions and the origin of negative $\delta^{13}C_{carb}$ excursions as well as recover redox conditions of ancient seawater, although in some sections correlations have been difficult to establish due to spatially limited outcrops, poor constraints on bathymetry-dependent facies variations, and low sampling resolution (Yang et al., 1999; Sawaki et al., 2010; Jiang et al., 2007, 2011; Zhu et al., 2013; Cremonese et al., 2013; Kikumoto et al., 2014; An et al., 2015; Cui et al., 2015; Zhou et al., 2017; Wang et al., 2018). As a result, the origin and timing of both EN2 and EN3, and their chronological order with respect to Ediacaran glaciation, remains ambiguous, which has led to the proposal of two possible models for Ediacaran subdivisions and correlation (Xiao et al., 2016). Further high resolution chemostratigraphic studies can contribute to enhance our understanding of the occurrence, order and causal relationships between chemo-oceanographic chemical variations and Ediacaran glaciation during this key geological period.

In this study, drill core samples of the Doushantuo Formation are used to ensure that the chemostratigraphy is complete, continuous, and studied at high-resolution as well as to minimize the influence of late oxidation and surface weathering. Previously published $\delta^{13}C_{carb}$, $\delta^{13}C_{org}$, $\delta^{15}N$ and $^{87}Sr/^{86}Sr$ stratigraphy are compiled and directly compared to new detailed chemostratigraphy of $\delta^{13}C$ and $^{87}Sr/^{86}Sr$. With this approach, the origin of Ediacaran negative $\delta^{13}C_{carb}$ excursions and their chemostratigraphic correlations are discussed.

2. Geological setting

The Ediacaran Yangtze platform in South China developed on a Neoproterozoic rifted continental margin that is believed to have started along the southeastern side of the Yangtze block at ca. 800 Ma (Wang and Li, 2003; Jiang et al., 2007). A passive margin setting is assumed to accommodate the post-glacial Ediacaran carbonate and siliciclastic rocks (Jiang et al., 2003a). Ediacaran sedimentary rocks are widely exposed around the Yangtze block and preserve a key biostratigraphic and chemostratigraphic record of the co-evolution of life and its environments in the Doushantuo and Dengying formations (Figure 1A, B; Zhou and Xiao, 2007; Zhu et al., 2007; Chen et al., 2014; Liu et al., 2014; Xiao et al., 2014; Cui et al., 2015).

Detailed facies analyses and palaeogeographic reconstructions based on more than twenty sections suggest that the Doushantuo Formation was deposited in three platform facies belts, as represented by 1) proximal inner shelf peritidal mixed carbonate and shale, 2) an intra-shelf lagoon containing mixed carbonate, phosphorite, and shale, and 3) an outer shelf shoal complex with increasing water depth from northwest to southeast (Figure 1C; Zhu et al., 2007; Jiang et al., 2011). The Doushantuo Formation was deposited in two stages. The first stage and, in particular, the couplet of cap carbonate and overlying black shale of the lower Doushantuo Formation indicates an open shelf/ramp depositional environment after the Nantuo glaciation. The second stage is characterized by its rimmed carbonate shelf with a shelf-margin barrier separating the intra-shelf lagoon from open ocean settings (Jiang et al., 2011). One of the most complete and continuous outcrops of the Doushantuo

Formation is exposed at the intra-shelf basin Jiulongwan section within the Yangtze Gorges area (Liu and Sha, 1963; Sawaki et al., 2010). Therein, the mixed shale and carbonate of the Doushantuo Formation have a total thickness of ca. 160 m and conformably overlie the Nantuo Formation, which is dominated by greenish diamictite with minor red sandstone beds interpreted to be glaciogenic sediments correlative with the late Cryogenian 'Marinoan glaciation' (Liu and Sha, 1963; Lang et al., 2018). The Doushantuo Formation at Jiulongwan is divisible into, in ascending order, Member 1 composed of cap dolostone, Member 2 dominated by black shale, Member 3 dominated by dolostone and Member 4 composed exclusively of black shale (with carbonate concretions). Conformably overlying the Doushantuo Formation is the Dengying Formation, which is mainly composed of mixed dolostone and limestone that can be divided into three members: the Hamajing, Shibantan and Baimatuo members, in ascending order (Zhu et al., 2003).

The outer-shelf Wangjiapeng section is well-represented in drill core No. WZK101, which is situated between the Jiulongwan section and the Yangjiaping section, with GPS coordinates of (30º31′36″N; 111º01′29″E) (Figure 1B). The Doushantuo Formation at Wangjiapeng begins with ca. 5 m of cap carbonate on top of the Nantuo glacial diamictite, succeeded by ca. 80 m of muddy dolostone intercalated with muddy limestone and shale, which is followed in turn by ca. 170 m of thick muddy limestone, muddy dolostone, shale and dolostone. Such lithological assemblage is similar to that occurring around Jiulongwan section where black shale or calcareous shale is also present, indicating that these two sections are adjacent and could have deposited in a similar sedimentary environment. At Wangjiapeng section, the Doushantuo/Dengying boundary can be identified by the thick-bedded dolostone at the bottom of the Dengying Formation. No radiometric ages have been obtained from these drill core samples. However, the depositional age of the Doushantuo Formation at Jiulongwan section is constrained to cover the interval between circa 635 Ma and 551 Ma by means of TIMS U-Pb dating of zircon grains from two interbedded tuff beds around the base of the Doushantuo Formation and close to the Doushantuo-Dengying Formation boundary (Condon et al., 2005) and Lu-Hf age of 584 ± 26 Ma and Pb-Pb age of 599.3 ± 4.2 Ma from the phosphorite of Doushantuo Formation (Barfod et al., 2002), which means that the Doushantuo Formation spans roughly 80 million years.

3. Analytical methods

3.1. Imaging analyses

Thin sections were prepared by cutting samples perpendicular to the bedding plane surface so as to detect typical internal microstructures under the Nikon Eclipse E800 Microscope equipped with a Nikon DS-Fi 1 camera using transmitted and reflected lights. This is because microtextures such as cemented grains and diagenetic pyrite are better observed in cross sections. The Zeiss 1555 VP-FESEM was utilized to detect minerals of micron to submicron meters. The SEM was specifically manipulated to get an optimal resolution at 50,000-200,000. It was tuned to an optimal working distance of 7-15 mm and a voltage of 10-20 kV.

3.2. Carbonate carbon and oxygen isotope analyses

In order to limit as far as possible influence of late-stage diagenetic alteration of carbonate minerals, penetration of carbonate/quartz veins and field outcrop weathering, 144 samples were taken from drill core at the Central South Institute of Metallurgical Geology, Yichang, China for $\delta^{13}C_{carb}$ and $\delta^{18}O_{carb}$ analyses. Carbonate $\delta^{13}C_{carb}$ and $\delta^{18}O_{carb}$ values were measured using a continuous gas flow mass spectrometer (Delta V Plus; Thermo Fischer Scientific Inc.) coupled to a carbonate reaction device (Gasbench II, Thermo Fischer Scientific Inc.) at the Atmosphere and Ocean Research Institute of The University of Tokyo. Powdered samples (~0.2 mg) were loaded into vials sealed with rubber septae. After replacing air in the vials with ultrapure He gas, carbonate was reacted with phosphoric acid at 72 °C to produce CO_2 gas. An automated needle was used to transfer the carbon dioxide analyte gas from the head space in a stream of ultrapure He gas, which was separated by gas chromatography and water removal with a Nafion trap before being introduced into the source of the isotope ratio mass spectrometer. Isotopic results are reported in the delta notation as per mil (‰) deviations from the V-PDB based on NBS-19. Based on repeated analyses of a $CaCO_3$ standard (JCt-1, Okai et al., 2002), reproducibility for $\delta^{13}C_{carb}$ and $\delta^{18}O_{carb}$ was 0.12‰ and 0.14‰ (n=11, 1σ), respectively.

3.3. Nitrogen and organic carbon isotope analyses

For nitrogen and organic carbon isotope analyses, the sediment samples were subjected to removal of carbonate and rinsing procedures before chemical analysis. About 200 mg of the powdered samples were digested in 10mL of 10 M HCl at 60˚C overnight. After centrifugation, the supernatant was removed, and the sediment rinsed with MQ water several times to remove residual acid. After drying at 60˚C overnight, the residual sample (~40-100 mg) was wrapped within a tin capsule with a combustion improver (WO_3). Nitrogen and carbon isotope ratios ($\delta^{15}N$ and $\delta^{13}C_{org}$) of the residual samples were measured by elemental analyzer (vario MICRO cube, elementar) connected to an isotope ratio mass spectrometry (IsoPrime100, IsoPrime, U.K.) coupled with combustion device (vario MICRO cube, elementar, Germany), installed at Atmosphere and Ocean Research Institute, The University of Tokyo, Japan. In this study, stable isotope compositions are expressed as δ values that were determined as a ratio of the heavy to light isotopes in the sample relative to the international standard reference materials by an equation:

$$\delta X(‰) = (R_{sample}/R_{standard}-1) \times 1000$$

where, X is the isotope ($^{13}C_{org}$ and ^{15}N) value in permil (‰) and R is the ratio of the heavy to light isotope of the sample (R_{sample}) and the international standard reference materials, namely N_2 air for $\delta^{15}N$ and Viem Pee Dee Belemnite for $\delta^{13}C_{org}$ ($R_{standard}$). The isotope ratios of nitrogen and carbon in the samples were calibrated against a commercial standard (L-alanine (SS13), Shoko Scientific), of which $\delta^{15}N$ and $\delta^{13}C_{org}$ are 13.7 ± 0.2‰ air and -19.6 ± 0.2‰ VPDB, respectively. The NIST SRM2976 (National Institute of Standards and Technology, USA) was analyzed for monitoring the instrumental condition during the course of analysis. Reproducibility for $\delta^{15}N$ and $\delta^{13}C_{org}$ (RSD of NIST 2976 repetition n = 6) was 0.27 and 0.28‰, respectively. Total Organic Carbon (TOC) and Total Nitrogen (TN) were not measured in this study so C/N ratios could not be obtained.

3.4. Strontium isotope analyses

Powdery samples were prepared from the 144 drill core samples. They were crushed into 200 mesh powder using an agate shatter box. The rock powders were dissolved in 2 M acetic acid at 70 ˚C overnight for chemical composition analysis. Dilute acetic acid was used in order to avoid dissolving the detrital silicate minerals. The acid-macerated samples were rinsed three times with Milli-Q water to remove strontium from the carbonate minerals. The supernatant was then centrifuged to separate insoluble residues followed by decantation and drying. Following the extraction of insoluble residues from sample solutions, dissolved samples were dried and then re-dissolved in 2 M nitric acid. After dilution by adding 2% nitric acid, an inductively coupled plasma-mass spectrometry (ICP-MS; Agilent 7700, Agilent Technologies) at Gakushuin University, Japan was used to obtain Al, Si, K, Mn, Fe, Rb, and Sr concentrations. The precision for these measurements is better than 3%. Any insoluble residue was deducted from the calculation of elemental concentrations. For more details please refer to Sawaki et al. (2010).

Strontium isotope analyses were selectively conducted on 40 drill core samples guided by detailed petrographic observations so as to characterize the primary isotopic compositions of seawater. In order to avoid the influence of isobaric interferences, Sr was chemically separated from coexisting matrix elements such as Rb by a chromatographic technique using Sr Resin (Eichrom Technologies, Incorporation) (Ohno and Hirata, 2007). Following dissolution in 2 M nitric acid, the samples were loaded onto ca. 0.25 ml of preconditioned Sr Spec column (i.d. 6 mm, height 10 mm, particle 50-100 um). Sr was eluted by 5 ml of 0.05 M nitric acid following removal of matrix elements by 5 ml of 7 M nitric acid and 3 ml of 2 M nitric acid.

The Sr isotope compositions of ^{86}Sr, ^{87}Sr, and ^{88}Sr were measured with a Nu plasma 500 MC-ICP-MS (Nu Instrument Ltd, Wrexham, Wales) at Gakushuin University, Japan. The analytical standard solution NIST SRM 987 was used to calibrate peak intensities of sample solutions to obtain the elemental abundances. The sample-standard bracketing technique was employed to improve the reproducibility of the measurements. All $^{87}Sr/^{86}Sr$ ratios of the Doushantuo samples were corrected by normalizing the $^{87}Sr/^{86}Sr$ isotope ratios relative to the NIST standard SRM 987, the $^{87}Sr/^{86}Sr$ ratio of which is 0.71025. Description of the mass discrimination effect has been detailed in previous studies (Ohno and Hirata, 2007; Ohno et al., 2008; Sawaki et al., 2010). The primary values of radiogenic $^{87}Sr/^{86}Sr$ isotope ratios were calculated from the minimum depositional ages (551 Ma) and Rb/Sr ratios by applying a half-life of 4.88×10^{10} years for ^{87}Rb.

4. Results

4.1. Petrography of the studied rock samples

A total of 144 drill core samples were collected with a sampling interval ranging from 0.8-1.6 m, which can be classified into five lithofacies (Figures 2-5). They are calcareous shale, dolostone, muddy dolostone, limestone, and muddy limestone, all of which exhibit a dark color. Chert veins occasionally occur in the limestone and muddy dolostone. Shale is found at the bottom, middle and upper parts of the Doushantuo Formation, and is mainly composed of clay minerals and feldspar with minor amounts of dolomite, apatite and pyrite (Figures 2A-B). Dolostone is found at the bottom, middle and top parts of the Doushantuo Formation, and is mainly composed of microcrystalline dolomite with minor amounts of calcite and pyrite (Figures 2C-D). The grain contour of dolomite is not so clear so it is not easy to assess the grain size. In contrast to dolomite, calcite shows a relatively bright BSE color and is present as pore-filling cement between dolomite crystals with a size commonly <10 μm.

Muddy dolostone occurs at lower, middle and upper part of the Doushantuo Formation, and is mainly composed of dolomite and calcite with minor amount of quartz and feldspar (Figures 3A-D). Some samples contain calcite veins that are generally 50-200 μm in width and oriented in various directions (Figure 3C). Dolomite generally shows a clear contour with a size range of 10-30 μm. Framboidal pyrites are abundant and fill pore spaces with a size range of typically <7 μm. Quartz grains are occasionally present with a size range of 25-30 μm. Limestone occurs in the middle-lower part of the Doushantuo Formation and is dominated by calcite with negligible amount of dolomite, apatite, pyrite and organic material (Figure 4). Neither calcite nor dolomite grain outlines are clear so individual grains are hard to recognize. Apatite grains, commonly 20-25 μm long, show a sub-rounded morphology intergrown with calcite. Some limestone samples contain chert veins that are generally 2-4 mm in width and oriented in various directions (Figure 4B). Like limestone, muddy limestone also occurs in the middle-lower part of the Doushantuo Formation and is dominated by calcite with minor amounts of dolomite, apatite and clay minerals (Figure 5). Calcite grain outlines are not so clear so individual grains are hard to recognize.

4.2. Geochemical compositions

Chemical and isotopic compositions of the 144 carbonate core samples are shown in Table 1 and plotted in Figure 6. Strontium isotope ($^{87}Sr/^{86}Sr$) values remain steady in a narrow range of 0.7080-0.7084 in the lower part of the succession, while they increase to the range of 0.7084-0.7090 with a maximum of 0.7094-0.7100 in the upper part (Figure 6). Rb/Sr ratios vary in the range of 10^{-5}-10^{-2} with 6-7 fluctuations in the lower part followed by a steady increase to 10^{-3}-10^{-2} in the lower part and drop to 10^{-4}-10^{-2} in the upper part. Mn/Sr ratios mainly vary in the range of 0.1-1 in the upper part, whereas they spread more widely in the range of 0.01-10 in the lower part. Mn contents first reach values around 1,000 ppm in the basal part and then decrease to around 100 ppm on the top, where two positive excursions punctuated by one negative excursion are recorded. Fe contents generally fluctuate between 1,000-10,000 ppm. Except for the lower part, Fe contents show covariation with Mn content. Decoupling occurs between Mn and Fe in the lower part.

Sr contents show generally steady levels in the range of 100-1,000 ppm throughout the succession except at the top where they drop to <100 ppm. Carbonate carbon isotope ($\delta^{13}C_{carb}$) values reveal two negative excursions in the middle-lower part with the lowest values of ca. -4‰ and ca. -6‰, respectively, but they mainly vary in the range of 4-8‰ in middle-upper part (Figure 6). In particular, the $\delta^{13}C_{carb}$ values in the basal cap dolostone at ca. 1-2 m sampling horizon vary from -4‰ to -2‰, slightly more positive than those observed in several worldwide Marinoan cap carbonates (Kennedy et al., 1998; Zhou and Xiao, 2007; Lu et al., 2013; Wang et al., 2014). The second negative excursion occurs in muddy dolostone of the middle Doushantuo Formation at ca. 200 m's stratigraphic horizon. Organic carbon isotope data ($\delta^{13}C_{org}$) mainly range between -30‰ and -28‰ with five data points >-28‰ at the bottom and five data points <-30‰ at the top of the section. The magnitude of carbon isotope fractionation ($\Delta\delta^{13}C$) can be approximated by comparing the measured carbonate carbon and organic carbon isotope values in individual samples. The $\Delta\delta^{13}C$ values mainly vary between 30‰ and 35‰ through most of the measured section, with the exception of a deceasing trend to 25-27‰ at the bottom and upper part (ca. 200 m horizon) of the measured section.

Only 131 out of the 144 samples produce meaningful $\delta^{15}N$ values because of low total organic carbon (TOC) and total nitrogen (TN) contents. The $\delta^{15}N$ values generally vary from 3‰ to 9‰, with an average of 5.6‰. Five samples fluctuates between 1‰ to 3‰, whereas one sample has a higher values of >9‰. The $\delta^{15}N$ profile is dividable into four intervals designated as NS1, NS2, NS3 and NS4 based on its temporal variations. $\delta^{15}N$ data from NS1 center around 5‰ to 7‰, accompanied by low $\delta^{13}C_{car}$ and relatively high $\delta^{13}C_{org}$. $\delta^{15}N$ values in interval NS2 display relatively low values from 2‰ to 7‰, with a maximum value nearly reaching up to 8‰, accompanied by relatively high $\delta^{13}C_{car}$ and low $\delta^{13}C_{org}$. In contrast, $\delta^{15}N$ values in interval NS3 show higher values varying from 5‰ to 9‰, with a maximum value nearly reaching 10‰, concurrent with slightly decreasingly $\delta^{13}C_{car}$ values and relatively invariant $\delta^{13}C_{org}$ values. $\delta^{15}N$ values in interval NS4 display decreasing values varying from 8‰ to 3‰, broadly concurrent with negative $\delta^{13}C_{car}$ excursion and relatively invariant $\delta^{13}C_{org}$ values. Carbonate oxygen isotope ($\delta^{18}O$) values range from -12 to 0‰ but is dominantly in the range of -8 to -2‰. A positive $\delta^{18}O$ excursion can be delineated in the upper Doushantuo Formation, which occurs simultaneously with positive $^{87}Sr/^{86}Sr$ and negative $\delta^{13}C_{carb}$ excursions.

5. Discussion

5.1. Evaluating the influence of post-depositional alteration and detrital components

Efforts were made to obtain primary $^{87}Sr/^{86}Sr$ values by evaluating the influence of post-depositional alteration and detrital components. Importantly, samples with feldspar and clay were avoided as far as possible from these analyses as these phases can lead to the mixing of this geochemical signal. Post-depositional processes tend to increase $^{87}Sr/^{86}Sr$ values as a result of the addition of ^{87}Sr induced by radioactive decay of ^{87}Rb (Walther, 2009). Because of the tendency of Rb to substitute for K, K-bearing silicates release ^{87}Sr into interstitial fluids where it may be taken up during growth or recrystallization of carbonates during diagenesis. Excess ^{87}Sr could also be supplied by radiogenic basinal or hydrothermal fluids during burial. Basically, $^{87}Sr/^{86}Sr$ ratios do not show any clear covariation with Mn/Sr and Rb/Sr ratios, while most Doushantuo samples are relatively Sr-rich (64-1,257 ppm with an average of 470 ppm) and have low Mn/Sr ratios (<0.9) and Rb/Sr ratios (<0.0109) (Figures 7A, B). Such low Rb/Sr ratios fall in the range of 0.001-0.01 proposed in previous studies for unaltered samples (Kaufman et al., 1993; Sawaki et al., 2010). Additionally, mixtures of different Sr sources would show a linear relationship in the $^{87}Sr/^{86}Sr$-Sr binary plot and high Sr content is generally interpreted to indicate good preservation of an original marine signature as shown by broad covariation in the Doushantuo Formation (Figure 7C; c.f. Fairchild et al., 2017). These lines of evidence suggest that post-depositional alteration processes on Sr isotopic ratios are negligible and thus that samples preserve primary $^{87}Sr/^{86}Sr$ ratios.

Sr isotope compositions in carbonate rocks are easily influenced by input of crustal detrital materials because of their tendency to possess radiogenic Sr isotopic compositions. This is particularly true if clay minerals and feldspar sourced from continental crust are involved which would increase Rb/Sr and $^{87}Sr/^{86}Sr$ ratios. Given that clay minerals and feldspars contain higher levels of Al, Si, K and Rb than carbonate minerals, the influence of such detrital component can be further examined by means of plotting binary correlations between $^{87}Sr/^{86}Sr$ ratios and Al, Si and K contents. The absence of any covariation between $^{87}Sr/^{86}Sr$ ratios and Rb/Sr, Al, Si and K contents suggests that the influence of clay minerals and feldspar on $^{87}Sr/^{86}Sr$ ratios is insignificant (Sawaki et al., 2010) and that most of the samples selected are suitable for preservation of primary oceanic signature (Figures 7D, E, F). While most Doushantuo samples in the current study were initially screened for suitability using geochemistry and SEM-based petrography, two samples show significantly higher $^{87}Sr/^{86}Sr$ values despite lower Mn/Sr and Rb/Sr ratios (DST271 and DST311) than others from the same stratigraphic unit. The presence of abundant cherty veins in sample DST271 suggests post-depositional hydrothermal influence from radiogenic basinal or hydrothermal fluids, whereas the presence of calcite veins in sample DST311 may be responsible for its higher $^{87}Sr/^{86}Sr$ values. These two samples are thus excluded from the discussion below.

The positive correlations between $\delta^{18}O$ and $\delta^{13}C$ values in carbonate rocks have been traditionally treated as an indication of diagenetic alteration by mixed fresh-marine waters (Allan and Matthews, 1982). The absence of such relationships in our samples (Figure 7g) thus represents evidence of the geochemical integrity of samples (Jacobsen and Kaufman, 1999; Fike et al., 2006; Halverson et al., 2007; Knauth and Kennedy, 2009). On the basis of experiments conducted on the shallow sub-surface of the Bahamas, positive correlations do not necessarily indicate meteoric alteration as it is not necessarily produced within the traditionally defined mixing zone, which means that there will be no correlation between $\delta^{18}O$ and $\delta^{13}C$ values in the altered vadose zone (Swart and Oehlert, 2018). In this regard, appraisal of diagenetic history should be based on combined geochemical evidence rather than $\delta^{18}O$ and $\delta^{13}C$ values alone. Post-depositional alteration would also cause a simultaneous shift of carbonate and organic $\delta^{13}C$ towards lower values (Oehlert and Swart, 2014). The lack of a covariation trend between carbonate and organic $\delta^{13}C$ values throughout the Wangjiapeng section, the presence of commonly low Mn/Sr (<1) ratios (Figure 6), the absence of positive correlations between $\delta^{18}O$ and $^{87}Sr/^{86}Sr$ ratios (Figure 7h), and the fact that our samples fall away from the meteoric alteration trend defined by comparing carbonate carbon and oxygen isotope abundances (Knauth and Kennedy, 2009) collectively indicate insignificant influence of secondary alteration. Therefore, the drill core samples preserve primary $\delta^{13}C_{carb}$ and $\delta^{18}O$ ratios. Authigenic carbonate would influence isotope compositions by precipitating highly ^{13}C-depleted calcite cement or relatively coarse-grained dolomite grains possessing less negative or sometimes slightly positive $\delta^{13}C$ values, a process that could produce $\delta^{13}C$ values less than $\leq$ -10‰ (Melezhik et al., 2005; Furuyama et al., 2016; Zhou et al., 2017). The commonly fine-grained texture of dolomite, the relatively high $\delta^{13}C$ values (> -6‰), the lack of any correlation between $\delta^{13}C_{carb}$ and $\delta^{18}O_{carb}$ values, and the gradual nature of $\delta^{13}C_{carb}$ trends, which are independent of lithological variability also point to an insignificant influence of diagenetic overprint for the negative carbon isotope excursions at Wangjiapeng section.

5.2. Chemostratigraphic correlation

Lithostratigraphic and sequence stratigraphic correlations have previously been attempted for most of the Yangtze platform sedimentary successions around shallow and deep water settings across the Nanhua Basin (Ader et al., 2009; Jiang et al., 2011; Wang et al., 2016). However, in some sections these correlations are hampered by depositional bathymetry-dependent facies variations, the absence of marker beds, or age diagnostic fossils for biostratigraphy (An et al., 2015; Zhou et al., 2017). Instead, chemostratigraphic correlations have been extensively attempted (Zhou and Xiao, 2007; Ader et al., 2009; Zhu et al., 2007, 2013). Three negative $\delta^{13}C_{carb}$ excursions have previously been proposed in the Doushantuo Formation (namely EN1, EN2, EN3, Jiang et al., 2007; Zhou and Xiao, 2007; McFadden et al., 2008; Sawaki et al., 2010), whereas five excursions (NI-1, NI-2, NI-3, NI-4, NI-5) are also proposed by others (Tahata et al.,2013) based on a chemostratigraphic study of two successive drill cores around the Wuhe-Aijiahe area around the Three Gorges. While the three major negative $\delta^{13}C_{carb}$ excursions (NI-1, NI-4, NI-5) are correlative with EN1, EN2 and EN3 (Lu et al., 2013; Wang et al., 2014; Cui et al., 2015; Pokrovsky and Bujakaite, 2015; Xiao et al., 2016), the other minor negative $\delta^{13}C_{carb}$ excursions (NI-2, NI-3) are fragmented or ambiguous as they could have been induced by post-depositional alteration processes (Jiang et al., 2007; Tahata et al., 2013). Carbon, oxygen, and strontium isotopes coupled with trace element analyses suggest that dolomite resting on the diamictite of the Nantuo Formation at the Wangjiapeng section is similar to the cap carbonates found around the Ediacaran Yangtze platform and other sections worldwide (Hoffman et al., 1998; Jiang et al. 2003b, 2006; Zhou and Xiao, 2007; Zhu et al., 2007). Thus the negative $\delta^{13}C_{carb}$ excursion correlates with EN1, which likely occurred globally following the Marinoan glaciation (Hoffman et al., 1998; Hoffman and Schrag, 2002).

The similar magnitude and duration of the upper negative $\delta^{13}C_{carb}$ excursions at the Wangjiapeng section suggest correlation with the adjacent Zhongling and Yangjiaping sections of Hunan Province (Figure 8; Cui et al., 2015; Furuyama et al., 2016). This means that the upper negative $\delta^{13}C_{carb}$ excursion at the Wangjiapeng section, like that at the Zhongling and Yangjiaping sections, could also be part of EN3 (EN3a, McFadden et al., 2008; Cui et al., 2015). Based on a high-resolution time-series trend of multiple chemostratigraphic proxies ($\delta^{13}C$-$\delta^{34}S$-$^{87}Sr/^{86}Sr$-Ce/Ce*), Cui et al. (2015) documented a negative $\delta^{13}C_{carb}$ excursion (as low as -10‰) at Yangjiaping section and correlate it with part of EN3 and the worldwide Shuram-Wonoka anomaly. Reexamination of the same section led Furuyama et al. (2016) to propose such highly negative $\delta^{13}C_{carb}$ excursions may have experienced diagenetic overprint, and that the newly obtained negative $\delta^{13}C_{carb}$ excursions (< -5‰) coupled with relatively high $^{87}Sr/^{86}Sr$ ratios could correlate with EN2. Furuyama et al. (2016) further argued that Cui et al. (2015)'s correlation is mainly based on placement of the Doushantuo/Dengying boundary in the middle of the sedimentary unit above the phosphorite, and their $^{87}Sr/^{86}Sr$ data lack higher ratios (0.7088-0.7090) typical of EN3 interval. After detailed petrographic and geochemical observations, Cui et al. (2016) proposed that Furuyama et al. (2016)'s correlation scheme is mainly based on a putative rise of $^{87}Sr/^{86}Sr$ ratios in the EN2 interval, measurement of which was conducted on muddy and silty dolostone with Mn/Sr >1 and total carbonate <60%. Both of these studies have contributed to our understanding of the chemostratigraphic correlation. A fair judgement is that Furuyama et al. (2016)'s work best explains the influence of diagenetic overprint on the original carbon isotope composition of seawater, whereas Cui et al. (2015, 2016)'s works adequately accounts for oxidizing conditions to provide adequate sulfate for the organic carbon to be remineralized producing the negative $\delta^{13}C_{carb}$ excursion. They both emphasized that this negative $\delta^{13}C_{carb}$ excursions links enhanced oxidative continental weathering that transports radiogenic strontium and sulfate to the Ediacaran ocean. For samples containing total carbonate <60%, it should be called muddy carbonate or calcaresous shale by definition. This means it must contain certain amount of feldspar and clay minerals, which could potentially lead to the higher $^{87}Sr/^{86}Sr$ ratios. Similarly, samples from the stratigraphic interval of upper negative $\delta^{13}C_{carb}$ excursions at the Wangjiapeng section have higher $^{87}Sr/^{86}Sr$ ratios ranging from 0.7084-0.7088, which could also result from analyses of feldspar and clay minerals given its dominant muddy dolomite composition.

Correlation of the upper negative $\delta^{13}C_{carb}$ excursions at the Wangjiapeng section with EN3 is also supported by the paired $\delta^{13}C_{carb}$-$\delta^{13}C_{org}$ trends. The upper negative $\delta^{13}C_{carb}$ excursion at Wangjiapeng section is typical of decoupled $\delta^{13}C_{carb}$-$\delta^{13}C_{org}$ with nearly invariable $\delta^{13}C_{org}$ values, which is similar to the EN3 documented from the Zhongling and Yangjiaping sections (Cui et al., 2015), and the EN3 described from the Jiulongwan section (McFadden et al., 2008). It shows a short occurrence (less than 10 m) with a lowest value of ca. -6‰, which seemingly cannot be easily correlated with EN3 at Jiulongwan section, where the excursion has a relatively longer duration (more than 40 m) and is more $\delta^{13}C$-depleted (lowest value of -10‰) (Jiang et al., 2007; McFadden et al., 2008; Tahata et al., 2013). The $\delta^{13}C$ variations in the upper Doushantuo Formation are more complex than previously recognized, which was demonstrated in recent detailed chemostratigraphic studies of multiple sections of the Doushantuo Formation in South China (Cui et al., 2015; Furuyama et al., 2016; Zhou et al., 2017). As Zhou et al. (2017) pointed out, the stratigraphic complexity of $\delta^{13}C_{carb}$ negative excursions in the upper Doushantuo Formation implies that some carbon isotope excursions are probably absent in some sections, particularly when they are dominated by non-carbonate rocks or compromised by sedimentary hiatus. This means the negative $\delta^{13}C_{carb}$ excursion from the upper part of Wangjiapeng, like those from the inner shelf Xiaofenghe section and outer shelf Zhongling and Yangjiaping sections (Cui et al., 2015), could also be part of EN3. EN3 with similar magnitude and duration has also been documented from other sections around the Huangling Anticline area (Zhou et al., 2017), and from worldwide sections in Oman (Fike et al., 2006) and Siberia (Pokrovsky and Bujakaite, 2015).

EN2 occurs within the 70-80 m stratigraphic horizons at the Jiulongwan section (Figure 9). Coincidently, negative $\delta^{13}C_{carb}$ excursion with magnitude and duration comparable to EN2 at the Jiulongwan section occurs also within the 70-80 m stratigraphic horizons at the Zhongling section. Given that the Wangjiapeng section is situated between the Jiulongwan and Zhongling sections, it can be envisaged that EN2 could have originally occurred somewhere around the 70-80 m stratigraphic horizon at the Wangjiapeng section but was later eroded away because of depositional hiatus. Unfortunately, the limited lateral extent of core samples and poor outcrops makes this hypothesis untestable for us to clearly define the stratigraphic position of the unconformity. The original thickness of the sedimentary units would have changed in response to faulting or folding related tectonic activities. Geographically, the Jiulongwan section is situated in the depocenter within an intra-shelf setting so theoretically it must have the largest thickness. However, the stratigraphic thickness at the Wangjiapeng section is 100 m thicker than that at the Jiulongwan section, which suggests potential stratigraphic repetition in the former possibly related to faulting activity. This is particularly possible for the structurally complex Wangjiapeng section.

Alternatively, the similar magnitude and duration means that the upper negative $\delta^{13}C_{carb}$ excursions at Wangjiapeng section could be correlated with EN2 within the Hushan-Dayukou, Baiguoyuan, Liuhuiwan, Miaohe, and Xiangdangping sections around the Three Gorges area as well as in Guizhou Province (Zhu et al., 2013). Nevertheless, absence of paired $\delta^{13}C_{carb}$-$\delta^{13}C_{org}$ values as well as $^{87}Sr/^{86}Sr$ ratios means that this correlation scheme requires future confirmation. Pending further geological and geochemical evidence, this problem remains open for discussion.

5.3. Genesis of EN3

The formation of such a negative $\delta^{13}C_{carb}$ anomaly (EN3) demands an additional flux of isotopically light dissolved inorganic carbonate (DIC), with several plausible sources of ^{13}C-depletion alkalinity proposed, including 1) flux of methane hydrates from an anoxic ocean that is enriched in dissolved organic carbon (Bjerrum and Canfield, 2011), 2) dissolved organic compounds (DOC) pool in the oceans (Rothman et al., 2003), 3) fossil organic substances exposed on continent (Kaufman et al., 2007), and 4) involvement of authigenic carbonates of anomalous isotopic composition formed via SRB-AOM in normal seawater precipitates (Schrag et al., 2013). The last possibility can be easily discounted as authigenic carbonates formed via SRB-AOM generally have extremely low $\delta^{13}C_{carb}$ values (<-30‰, VPDB) despite mixing with normal seawater precipitates (Zhou et al., 2016).

Remineralization of DOC pool is a possible way to account for the non-covariation trend between $\delta^{13}C_{carb}$ and $\delta^{13}C_{org}$ values and a steady, invariable trend of $\delta^{13}C_{org}$ values during the $\delta^{13}C_{carb}$ excursion (Rothman et al., 2003). This is because a relatively small DIC pool would be more easily influenced by isotope variations if the DOC pool was large, and accordingly this would decouple carbonate and organic carbon isotope signatures. Based on the $\delta^{13}C_{carb}$ study of four sections deposited in basin to slope to platform settings, Jiang et al. (2007) ascribed the EN2 and EN3 to the remineralization of an oceanic DOC pool by means of sulfate reduction. This model was accepted by Ishikawa et al. (2013) who associated the decoupling of $\delta^{13}C_{carb}$ and $\delta^{13}C_{org}$ with the presence of a huge DOC pool which lasts from terminal Proterozoic to Early Cambrian. The spatial limitation of paired $\delta^{13}C_{carb}$-$\delta^{13}C_{org}$ data restricted the wide application of a large DOC model. Subsequent research suggests that the decoupling of $\delta^{13}C_{carb}$ and $\delta^{13}C_{org}$ could depend on lithology and the decoupled $\delta^{13}C_{carb}$ and $\delta^{13}C_{org}$ pattern could have resulted from involvement of recycled/detrital organic carbon (Jiang et al., 2010, 2012; Johnston et al., 2012). Wang et al. (2016) proposed the growth of a DOC reservoir from Ediacaran to the the early Paleozoic is episodic, and the spatial $\delta^{13}C_{org}$ variations does not necessarily link the decoupled $\delta^{13}C_{carb}$-$\delta^{13}C_{org}$ with direct buffering of a DOC reservoir but possibly with recycling of organic materials derived from chemoautotrophs and methanotrophs. The presence of nearly invariable $\delta^{13}C_{org}$ values and decoupled $\delta^{13}C_{carb}$-$\delta^{13}C_{org}$ signals in EN3 from the Doushantuo Formation at the Wangjiapeng, Jiulongwan (McFadden et al., 2008), Zhongling and Yangjiaping sections (Cui et al., 2015) suggest that EN3 possibly resulted from the remineralization of an oceanic DOC pool via sulfate reduction. However, the possibility that the decoupled $\delta^{13}C_{carb}$ and $\delta^{13}C_{org}$ pattern have resulted from involvement of recycled/detrital organic carbon cannot be totally discounted given the dominant muddy dolomite composition from the EN3 interval at the Wangjiapeng section.

As with previous studies (Sawaki et al., 2010; Tahata et al., 2013; Furuyama et al., 2016), association of the negative $\delta^{13}C_{carb}$ excursion in EN3 with remineralization of reduced carbon sources induced by the Gaskiers glaciation is favored at Wangjiapeng section. The limestone-dominated carbonate of EN3 around the Three Gorges sections have a dominant ^{18}O spread range of -8 to -4‰ (Tahata et al., 2013). The $\delta^{18}O_{carb}$ values of muddy dolostone of EN3 at the Wangjiapeng section range between -4 to 0‰. Considering the differential fractionation factors between calcite and dolomite, i.e. the former being 2-3‰ more depleted in ^{18}O than the latter (Vasconcelos et al., 2005), the nadir values of EN3 between the Three Gorges and Wangjiapeng sections would be indistinguishable, both of which may have resulted from a common glacial influence.

Hydrothermal influx from oceanic crust and riverine input from continental weathering are the two dominant sources of marine manganese and iron, the contents of which are generally influenced by redox conditions of the water column (Sawaki et al., 2010; Tagliabue et al., 2010). Mn^{2+} and Fe^{2+} are enriched in anoxic conditions where they form solid solutions in carbonate minerals, whereas under oxic conditions Mn^{2+} and Fe^{2+} tend to be oxidized forming oxide and oxyhydroxide nanoscopic minerals. The decrease of Mn and Fe contents of Wangjiapeng sediments coincides with EN3, and also significantly decrease after EN3, which further indicates overall oxygen-poor condition of ambient seawater during the Gaskiers glaciation because of oxidative decay of the DOC and an abrupt increase of the oxygen content following the glaciation (Sawaki et al., 2010).

Normal marine production is typical of a state of equilibrium among nitrate assimilation, N_2 fixation and denitrification, achieving near modern oceanic values in the range of +2‰ to +9‰ (Cremonese et al., 2013; Kikumoto et al., 2014; Wang et al., 2017, 2018). The $\delta^{15}N$ values from the Wangjiapeng section are mostly scattered from +3‰ to +9‰ (Figure 6), suggestive of typical modern oceanic values. It is worth noting that $\delta^{15}N$ values of the Doushantuo Formation at Wangjiapeng section are broadly consistent with those of the Doushantuo Formation at Three Gorges section (Kikumoto et al., 2014), Yangjiaping section (Ader et al., 2014) and the Lantian Formation (equivalent of Doushantuo Formation) at Lantian section (Wang et al., 2017) (Figure 10). In particular, the Doushantuo Formation at Wangjiapeng section (average $\delta^{15}N$ = 5.1‰) has statistically consistent values with the Lantian Formation (average $\delta^{15}N$ = 5.3‰) within errors, but higher values than the Doushantuo Formation at Yangtze Gorges area (average $\delta^{15}N$ = 4.8‰) and Yangjiaping (average $\delta^{15}N$ = 4.4‰) of South China with difference in average $\delta^{15}N$ values within 1‰. From the perspective of $\delta^{15}N$ values, the Doushantuo and Lantian formations are broadly similar to the Ediacaran successions in Svalbard ($\delta^{15}N$ = 5.1 ± 0.5‰) and Brazil (5.1 ± 2.0‰ in Brazil), but differ from that in northwestern Canada ($\delta^{15}N$ = 2.9 ± 0.6‰) (Wang et al., 2017 and literatures therein). As Wang et al. (2017) pointed out, the overall similarity in $\delta^{15}N$ values of the Doushantuo and Lantian formations in South China indicate the nitrogen cycle was influenced by basinal rather than local factors despite the requirement of further solid evidence.

Microbial denitrification leads to partial reduction of nitration into N_2/N_2O. This would produce large isotopic fractionation and resultant ^{15}N-enrichment in nitrate followed by assimilation into biomass (Sigman et al., 2009; Cremonese et al., 2013). Accordingly, higher $\delta^{15}N$ values are generally interpreted to represent an oxygen-depleted condition where supply of nitrate into the ocean was depressed by denitrification or assimilation, whereas lower $\delta^{15}N$ values are regarded as an indication of relatively oxygenated/oxygen-rich depositional setting where supply of nitrate exceeded denitrification or assimilation (Cremonese et al., 2013; Kikumoto et al., 2014; Wang et al., 2018). Some $\delta^{15}N$ values dropped from +8‰ to nearly +3‰ during NS4 (broadly coeval with EN3/Shuram $\delta^{13}C_{carb}$ excursion). Shift of $\delta^{15}N$ to lower values during this interval is interpreted to represent an increasing nitrate reservoir under oxygenated/oxygen-rich depositional setting, which is consistent with the decreasing trend of Mn and Fe contents. Such a decreasing trend is consistent with the gradual oxidation of Ediacaran oceans (Fike et al., 2006; McFadden et al., 2008; Kikumoto et al., 2014). Decrease of the $\delta^{15}N_{TN}$ value occurred near synchronously with the Shuram $\delta^{13}C_{carb}$ excursion, before which a large organic carbon pool existed in the ocean as evidenced by the decoupled $\delta^{13}C_{carb}$ and $\delta^{13}C_{org}$ values. Coupling of $\delta^{13}C_{carb}$ and $\delta^{13}C_{org}$ values resumed following the termination of the Shuram excursion, which may indicate oxidation of the large organic carbon pool in the ocean (Kikumoto et al., 2014). In this regard, the synchronous presence of negative $\delta^{13}C_{carb}$ excursions combined with positive $\delta^{18}O$ shifts, decrease of Mn and Fe contents and decrease of $\delta^{15}N$ values together point to transition from low oxygen to oxygen rich environment possibly related to the melting of Ediacaran glaciation.

Global cooling can induce global regression and enhance the oxidative decay of exposed marine sediments rich in organic matter. Continental weathering can increase as sea levels would be significantly lowered, and therefore marine sediments on continental shelves would be widely exposed as a result of glaciation-induced regression (Sawaki et al., 2010). Draining of terrestrial radiogenic Sr-enriched rocks such as precursor carbonate ($^{87}Sr/^{86}Sr$~0.705-0.709) and/or silicate rocks ($^{87}Sr/^{86}Sr$>0.715) by means of river water flux would induce an increase of radiogenic Sr contents and a corresponding increase of $^{87}Sr/^{86}Sr$ (Banner, 2004; Pokrovsky and Bujakaite, 2015). As such, increased $^{87}Sr/^{86}Sr$ ratios during this interval are generally associated with enhanced delivery of radiogenic ^{87}Sr that originated from rapid continental weathering (Sawaki et al., 2010; Wang et al., 2014; Cui et al., 2015; Furuyama et al., 2016). Enhanced, post-glacial, continental weathering and erosion increase the influx of sulfate and phosphorus into the ocean (Sawaki et al., 2010; Papineau, 2010). Influx of nutrients contributed to primary productivity producing dissolved oxygen (She et al., 2014), interactions of which with reduced carbon sources in the deep ocean would have induced the oxidation of organic matter and therefore produce ^{12}C-enriched dissolved inorganic carbon (DIC) in seawater. Meanwhile, such negative $\delta^{13}C_{carb}$ anomaly would be enhanced as a result of remineralization of DOC by means of active sulfate reduction (Halverson and Hurtgen, 2007). As such, EN3 in the upper Doushantuo Formation at Wangjiapeng is probably best ascribed to oxygenation and remineralization of biomass, which produced ^{13}C-depleted DIC.

This study detected another distinct increase of $\delta^{13}C_{carb}$ values at ca. 50 m stratigraphic horizon (labelled EP in Figure 6). Such short-term positive $\delta^{13}C_{carb}$ coincides with the decrease of $\delta^{18}O$ and $\delta^{15}N$ values, Rb/Sr and Mn/Sr ratios as well as Mn and Fe contents. In particular, the widespread range of $\delta^{15}N$ values (+2‰ to +8‰) during this interval were probably formed via an aerobic nitrogen cycle in a relatively stable nitrate pool where partial water column denitrification might occur (Wang et al., 2018). The transition of higher $\delta^{15}N$ to lower $\delta^{15}N$ values may be induced by degradation of particulate organic matter (POM) when POM sinks quickly (Sigman et al., 2009). Rapid sinking of POM would leave the formation of ^{13}C-enriched carbonate. Zooplankton would induce the effective sinking of organic matter by means of producing fecal pellets despite its rarity in the Ediacaran ocean.

6. Conclusions

An integrated sequence- and chemo-stratigraphic study of the Ediacaran Doushantuo Formation carbonate platform around western Hubei Province reveals two negative $\delta^{13}C_{carb}$ excursions (EN1 and EN3) at two stratigraphic levels. The absence of positive covariation between $\delta^{13}C$ and $\delta^{18}O$ values and $^{87}Sr/^{86}Sr$ ratios, and presence of low Mn/Sr (<1) ratios indicate negligible influence of secondary alteration, and thus confirm that the core samples preserve primary $\delta^{13}C_{carb}$ and $\delta^{18}O$ ratios. In combination with previously published chemostratigraphic data from Yangtze Platform and Northern India, the two stratigraphic levels display remarkable lateral $\delta^{13}C_{carb}$ consistency, which thus indicates they are related to open marine environments. The stratigraphic complexity of $\delta^{13}C_{carb}$ negative excursions in the upper Doushantuo Formation means that some carbon isotope excursions are probably absent in some sections, which means that only EN1 and EN3 are present and that EN2 is missing at the Wangjiapeng section.

The synchronous presence of negative $\delta^{13}C_{carb}$ excursions combined with positive $\delta^{18}O$ shifts and decrease of Mn and Fe contents and $\delta^{15}N$ values during EN3 point to a common glacial influence. EN3 recorded in the upper Doushantuo Formation at Wangjiapeng can probably be ascribed to remineralization of a dissolved organic carbon (DOC) reservoir producing ^{13}C-depleted DIC, as evidenced by the invariable $\delta^{13}C_{org}$ values and decoupled $\delta^{13}C_{carb}$-$\delta^{13}C_{org}$ characteristics. Ediacaran glaciation caused a sea level fall, prompting more continental shelf to be exposed. Increased $^{87}Sr/^{86}Sr$ values during this interval are generally associated with enhanced delivery of radiogenic ^{87}Sr that originated from continental weathering, which together with sulfate and phosphate was brought into the ocean via surface runoff.

Acknowledgements

Editor Guochun Zhao and associate editor Shuhai Xiao are thanked for handling this manuscript. Ganqing Jiang and two anonymous reviewers are thanked for their critical and constructive comments, which have improved the scientific quality of this manuscript. Beneficial discussions with Xuelei Chu were acknowledged. Graham Shields is thanked for polishing the writing. This work was supported by National Science of Foundation of China (41673016) and Japanese Society for the Promotion of Science Fellowship (Grant15F15330).

References

Ader, M., Macouin, M., Trindade, R.I.F., Hadrien, M.H., Yang, Z., Sun, Z., Besse, J., 2009. A multilayered water column in the Eidacaran Yangtze platform? Insights from carbonate and organic matter paired $\delta^{13}C$. Earth and Planetary Science Letters, 288, 213–227.

Ader, M., Sansjofre, P., Halverson, G.P., Busigny, V., Trindade, R.I.F., Kunzmann, M., Nogueira, A.C.R., 2014. Ocean redox structure across the Late Neoproterozoic Oxygenation Event: A nitrogen isotope perspective. Earth and Planetary Science Letters, *396*, 1–13.

Allan, J.R., Matthews, R.K., 1982. Isotope signatures associated with early meteoric diagenesis. Sedimentology, 29, 797–817.

An, Z.H., Jiang, G.Q., Tong, J.N., Tian, L., Ye, Q., Song, H.J., 2015. Stratigraphic position of the Ediacaran Miaohe biota and its constrains on the age of the upper Doushantuo $\delta^{13}C$ anomaly in the Yangtze Gorges area, South China. Precambrian Research, 271, 243–253.

Banner, J.L., 2004. Radiogenic isotopes: systematics and applications to Earth surface processes and chemical stratigraphy. Earth Science Review, 65, 141–194.

Barfod, G.H., Albarede, F., Knoll, A.H., Xiao, S.H., Telouk, P., Frei, R., Baker, J., 2002. New Lu-Hf and Pb-Pb age constraints on the earliest animal fossils. Earth and Planetary Science Letters, 201, 203–212.

Bjerrum, C.J., Canfield, D.E., 2011. Towards a quantitative understanding of the late Neoproterozoic carbon cycle. Proceedings of National Academy of Sciences, U.S.A., 108, 5542–5547.

Bowring, S.A., Myrow, P.M., Landing, E., Ramezani, J., 2003. Geochronological constraints on terminal Neoproterozoic events and the rise of metazoans. Geophysical Research Abstracts, 5, 13219.

Bristow, T.F., Grotzinger, J.P., 2013. Sulfate availability and the geological record of cold seep deposits. Geology, 41, 811–814.

Bristow, T.F., Kennedy, M.J., 2008. Carbon isotope excursions and the oxidant budget of the Ediacaran atmosphere and ocean. Geology, 36, 863–866.

Burns, S.J., Haudenschild, U., Matter, A., 1994. The strontium isotopic composition of carbonates from the late Precambrian (~560-540 Ma) Huqf Group of Oman. Chemical Geology, 111, 269–282.

Calver, C.R., 2000. Isotope stratigraphy of the Ediacarian (Neoproterozoic III) of the Adelaide Rift Complex, Australia, and the overprint of water column stratification. Precambrian Research, 100, 121–150.

Campbell, K.A., 2006. Hydrocarbon seep and hydrothermal vent paleoenvironments and paleontology: past developments and future research directions. Palaeogeography, Palaeoclimatology, Palaeoecology, 232, 362–407.

Chen, Z., Zhou, C.M., Xiao, S.H., Wang, W., Guan, C.G., Hua, H., Yuan, X.L., 2014. New Ediacara fossils preserved in marine limestone and their ecological implications. Scientific Report, 4, DOI: 10.1038/srep04180.

Condon, D., Zhu, M., Bowring, S., Wang, W., Yang, A., Jin, Y., 2005. U–Pb ages from the Neoproterozoic Doushantuo Formation, China. Science, 308, 95–98.

Cremonese, L., Shields-Zhou, G., Struck, U., Ling, H.-F., Och, L., Chen, X., Li, D., 2013. Marine biogeochemical cycling during the early Cambrian constrained by a nitrogen and organic carbon isotope study of the Xiaotan section, South China. *Precambrian Research,* 225, 148–165.

Cui, H., Kaufman, A.J., Xiao, S.H., Zhu, M.Y., Zhou, C.M., Liu, X.M., 2015. Redox architecture of an Ediacaran ocean margin: Integrated chemostratigraphic ($\delta^{13}C$-$\delta^{34}S$-$^{87}Sr/^{86}Sr$-Ce/Ce*) correlation of the Doushantuo Formation, South China. Chemical Geology, 405, 48–62.

Cui, H., Xiao, S., Zhou, C., Peng, Y., Kaufman, A.J., Plummer, R.E., 2016. Phosphogenesis associated with the Shuram Excursion: petrographic and geochemical observations from the Ediacaran Doushantuo Formation of South China. Sedimentary Geology, 341, 134–146.

Fike, D.A., Grotzinger, J.P., Pratt, L.M., Summons, R.E., 2006. Oxidation of the Ediacaran Ocean. Nature, 444, 744–747.

Furuyama, S., Kano, A., Kunimitsu, Y., Ishikawa, T., Wang, W., 2016. Diagenetic overprint to a negative carbon isotope anomaly associated with the Gaskiers glaciation of the Ediacaran Doushantuo Formation in South China. Precambrian Research, 276, 110–122.

Guo, Q., Liu, C., Strauss, H., Goldberg, T., Zhu, M., Pi, D., Wang, J., 2006. Organic carbon isotope geochemistry of the Neoproterozoic Doushantuo Formation, South China. Acta Geologica Sinica, 80, 670–683.

Grey, K., Walter, M.R., Calver, C.R., 2003. Neoproterozoic biotic divesification: Snowball Earth or aftermath of the Acraman impact? Geology, 31, 459–462.

Grotzinger, J.P., Knoll, A.H., 1995. Anomalous carbonate precipitates: is the Precambrian the key to the Permian? Palaios, 10, 578–596.

Halverson, G.P., Dudás, F.Ö., Maloof, A.C., Bowring, S.A., 2007. Evolution of the $^{87}Sr/^{86}Sr$ composition of Neoproterozoic seawater. Palaeogeography, Palaeoclimatology, Palaeoecology, 256, 103–129.

Halverson, G.P., Hoffman, P.F., Schrag, D.P., Maloof, A.C., Rice, A.H.N., 2005. Toward a Neoproterozoic composite carbon-isotope record. Geological Society of America Bulletin, 117, 1181–1207.

Halverson, G.P., Hurtgen, M.T., 2007. Ediacaran growth of the marine sulfate reservoir. Earth and Planetary Science Letters, 263, 32–44.

HBGMR (Hubei Bureau of Geology and Mineral Resources), 1988. Memoir on Regional Geology of Hubei Province. Geological Publishing House, Beijing, 705 pp (in Chinese with English Abstract).

Hoffman, P.F., Kaufman, A.J., Halverson, G.P., Schrag, D.P., 1998. A Neoproterozoic Snowball Earth. Science, 281, 1342–1346.

Hoffman, P.F., Schrag, D.P., 2002. The Snowball Earth hypothesis: testing the limits of global change. Terra Nova, 14, 129–155.

Hoffman, P.F., Li, Z.X., 2009. A palaeogeographic context for Neoproterozoic glaciations. Palaeogeography, Palaeoclimatology, Palaeoecology, 277, 158–172.

Jacobsen, S.B., Kaufman, A.J., 1999. The Sr, C and O isotopic evolution of Neoproterozoic seawater. Chemical Geology, 161, 37–57.

Jiang, G.Q., Christie-Blick, N., Kaufman, A.J., Banerjee, D.M., Rai, V., 2002. Sequence stratigraphy of the Neoproterozoic Infra Krol Formation and Krol Group, Lesser Himalaya, India. Journal of Sedimentary Research, 72, 524–542. Jiang, G.Q., Sohl, L.E., Christie-Blick, N., 2003a. Neoproterozoic stratigraphic comparison of the Lesser Himalaya (India) and Yangtze Block (South China): paleogeographic implications. Geology, 31, 917–920.

Jiang, G.Q., Kennedy, M.J., Christie-Blick, N., 2003b. Stable isotopic evidence for methane seeps in Neoproterozoic postglacial cap carbonates. Nature, 426, 822–826. Jiang, G.Q., Kennedy, M.J., Christie-Blick, N., Wu, H.C., Zhang, S.H., 2006. Stratigraphy, sedimentary structures, and textures of the late Neoproterozoic Doushantuo cap carbonate in South China. Journal of Sedimentary Research, 76, 978–995.

Jiang, G.Q., Kaufman, A.J., Christie-Blick, N., Zhang, S., Wu, H., 2007. Carbon isotope variability across the Ediacaran Yangtze platform in South China: implications for a large surface-to-deep ocean $\delta^{13}C$ gradient. Earth and Planetary Science Letters, 261, 303–320.

Jiang, G.Q., Shi, X.Y., Zhang, S.H., Wang, Y., Xiao, S.H., 2011. Stratigraphy and paleogeography of the Ediacaran Doushantuo Formation (ca. 635-551 Ma) in South China. Gondwana Research, 19, 831–849.

Kaufman, A.J., Jacobsen, S.B., Knoll, A.H., 1993. The Vendian record of Sr and C isotopic variations in seawater: implications for tectonics and paleoclimate. Earth and Planetary Science Letters, 120, 409–430.

Kaufman, A.J., Jiang, G.Q., Christie-Blick, N., Banerjee, D.M., Rai, V., 2006. Stable isotope record of the terminal Neoproterozoic Krol platform in the Lesser Himalayas of northern India. Precambrian Research, 147, 156–185.

Kaufman, A.J., Corsetti, F.A., Varni, M.A., 2007. The effect of rising atmospheric oxygen on carbon and sulfur isotope anomalies in the Neoproterozoic Johnnie Formation, Death Valley, USA. Chemical Geology, 237, 47–63.

Kennedy, M.J., Runnegar, B., Prave, A.R., Hoffmann, K.H., Arthur, M.A., 1998. Two or four Neoproterozoic glaciations? Geology, 26, 1059–1063.

Kikumoto, R., Tahata, M., Nishizawa, M., Sawaki, Y., Maruyama, S., Shu, D., Han, J., Komiya, T., Takai, K., Ueno, Y., 2014. Nitrogen isotope chemostratigraphy of the Ediacaran and Early Cambrian platform sequence at Three Gorges, South China. *Gondwana Research,* 25, 1057–1069.

Knauth, L.P., Kennedy, M.J., 2009. The late Precambrian greening of the Earth. Nature, 460, 728–732.

Lan, Z.W., Chen, Z.Q., 2012. Exceptionally preserved microbially induced sedimentary structures from the Ediacaran post-glacial successions in the Kimberley region, northwestern Australia. Precambrian Research, 200-203, 1–25.

Lang, X.G., Chen, J.T., Cui, H., Man, L., Huang, K.J., Fu, Y., Zhou, C.M., Shen, B., 2018. Cyclic cold climate during the Nantuo Glaciation: Evidence from the Cryogenian Nantuo Formation in the Yangtze Block, South China. Precambrian Research, 310, 243–255.

Li, C., Love, G.D., Lyons, T.W., Fike, D.A., Sessions, A.L., Chu, X.L., 2010. A stratified redox model for the Ediacaran Ocean. Science, 328, 80–83.

Liu, H.Y., Sha, Q.A., 1963. Some problems on the Sinian system of the Yi Chang Gorge districts of the Yangtze River. Scientia Geologica Sinica, 4, 177–188.

Liu, P.J., Xiao, S.H., Yin, C.Y., Chen, S.M., Zhou, C.M., Li, M., 2014. Ediacaran acanthomorphic acritarchs and other micro fossils from chert nodules of the upper Doushantuo Formation in the Yangtze Gorges area, South China. Journal of Paleontology, 88, 1–139.

Lu, M., Zhu, M.Y., Zhang, J.M., Shields-Zhou, G., Li, G.X., Zhao, F.C., Zhao, X., Zhao, M.J., 2013. The DOUNCE event at the top of the Ediacaran Doushantuo Formation, South China: broad stratigraphic occurrence and non-diagenetic origin. Precambrian Research, 225, 86–109.

McCall, G.J.H., 2006. The Vendian (Ediacaran) in the geological record: enigmas in geology's prelude to the Cambrian explosion. Earth Science Review, 77, 1–229.

McFadden, K.A., Huang, J., Chu, X.L., Jiang, G.Q., Kaufman, A.J., Zhou, C.M., Yuan, X.L., Xiao, S.H., 2008. Pulsed oxidation and biological evolution in the Ediacaran Doushantuo Formation. Proceedings of National Academy of Sciences, 105, 3197–3202.

Melezhik, V., Fallick, A.E., Pokrovsky, B.G., 2005. Enigmatic nature of thick sedimentary carbonates depleted in ^{13}C beyond the canonical mantle value: the challenges to our understanding of the terrestrial carbon cycle. Precambrian Research, 137, 131–165.

Muscente, A.D., Hawkins, A.D., Xiao, S.H., 2015. Fossil preservation through phosphatization and silicification in the Ediacaran Doushantuo Formation (South China): a comparative synthesis. Palaeogeography, Palaeoclimatology, Palaeoecology, 434, 46–62.

Myrow, P.M., Kaufman, A.J., 1999. A newly discovered cap carbonate above Varanger-age glacial deposits in Newfoundland, Canada: Journal of Sedimentary Research, 69, 784–793.

Oehlert, A.M., Swart, P.K., 2014. Interpreting carbonate and organic carbon isotope covariance in the sedimentary record. Nature Communications, 5, 1–7.

Ohno, T., Hirata, T., 2007. Simultaneous determination of mass-dependent isotopic fractionation and radiogenic isotope variation of strontium in geochemical samples by MC-ICP-MS. Analytical Sciences, 23, 1275–1280.

Ohno, T., Komiya, T., Ueno, Y., Hirata, T., Maruyama, S., 2008. Determination of $^{88}Sr/^{86}Sr$ mass-dependent isotopic fractionation and radiogenic isotope variation of $^{87}Sr/^{86}Sr$ in the Neoproterozoic Doushantuo Formation. Gondwana Research, 14, 126–133.

Okai, T., Suzuki, A., Kawahata, H., Terashima, S., Imai, N., 2002. Preparation of a new geological survey of Japan geochemical reference material: Coral JCp-1. Geostand Newsletters, 26, 95–99.

Palmer, M., Edmond, J., 1992. Controls over the strontium isotope composition of river water. Geochimica et Cosmochimica Acta, 56, 2099–2111.

Papineau, D., 2010. Global Biogeochemical Changes at Both Ends of the Proterozoic: Insights from Phosphorites. Astrobiology, 10, 165–181.

Pierrehumbert, R.T., 2004. High levels of atmospheric carbon dioxide necessary for the termination of global glaciation. Nature, 429, 646–649.

Pu, J.P., Bowring, S.A., Ramezani, J., Myrow, P., Raub, T.D., Landing, E., Mills, A., Hodgin, E., Macdonald, F.A., 2016. Dodging snowballs: Geochronology of the Gaskiers glaciation and the first appearance of the Ediacaran biota. Geology, 44, 955–958.

Pokrovsky, B.G., Bujakaite, M.I., 2015. Geochemistry of C, O, and Sr isotopes in the Neoproterozoic carbonates from the southwestern Patom paleobasin, southern Middle Siberia. Lithology and Mineral Resources, 50, 144–169.

Rothman, D.H., Hayes, J.M., Summons, R., 2003. Dynamics of the Neoproterozoic carbon cycle. Proceedings of National Academy of Sciences U.S.A., 100, 8124–8129.

Sawaki, Y., Ohno, T., Tahata, M., Komiya, T., Hirata, T., Maruyama, S., Windley, B.F., Han, J., Shu, D.G., Li, Y., 2010. The Ediacaran radiogenic Sr isotope excursion in the Doushantuo Formation in the Three Gorges area, South China. Precambrian Research, 176, 46–64.

Schrag, D.P., Higgins, J.A., Macdonald, F.A., Johnston, D.T., 2013. Authigenic carbonate and the history of the global carbon cycle. Science, 339, 540–543.

She, Z.B., Strother, P., Papineau, D., 2014. Terminal Proterozoic cyanobacterial blooms and phosphogenesis documented by the Doushantuo granular phosphorites II: Microbial diversity and C isotopes. Precambrian Research, 251, 62–79.

Shields, G., 2007. A normalised seawater strontium isotope curve: possible implications for Neoproterozoic-Cambrian weathering rates and the further oxygenation of the Earth. eEarth, 2, 35–42.

Shields-Zhou, G., Och, L., 2011. The case for a Neoproterozoic Oxygenation Event: geochemical evidence and biological consequences. GSA Today, 21, 4–11.

Sigman, D.M., Karsh, K.L., Casciotti, K.L., 2009. Ocean process tracers: Nitrogen isotopes in the ocean. Encyclopedia of ocean science. Elsevier, Amsterdam, pp. 4138–4153.

Swart, P.K., Oehlert, A.M., 2018. Reviese interpretations of stable C and O patterns in carbonate rocks resulting from meteoric diagenesis. Sedimentary Geology, 364, 14–23.
Tagliabue, A., Bopp, L., Dutay, J.C., Bowie, A.R., Chever, F., Jean-Baptiste, P., Bucciarelli, E., Lannuzel, D., Remenyi, T., Sarthou, G., Aumont, O., Gehlen, M., Jeandel, C., 2010. Hydrothermal contribution to the oceanic dissolved iron inventory. Nature Geoscience, 3, 252–256.
Tahata, M., Ueno, Y., Ishikawa, T., Sawaki, Y., Murakami, K., Han, J., Shu, D., Li, Y., Guo, J., Yoshida, N., Komiya, T., 2013. Carbon and oxygen isotope chemostratigraphies of the Yangtze platform, South China: Decoding temperature and environmental changes through the Ediacaran. Gondwana Research, 23, 333–353.
Vasconcelos, C., McKenzie, J.A., Warthmann, R., Bemasconi, S.M., 2005. Calibration of the $\delta^{18}O$ paleothermometer for dolomite precipitated in microbial culturesand natural environments. Geology, 33, 317–320.
Walther, J.V., 2009. "Rubidium–Strontium Systematics". *Essentials of geochemistry*. Jones & Bartlett Learning, pp. 383–385.
Wan, B., Yuan, X.L., Chen, Z., Guan, C.G., Pang, K., Tang, Q., Xiao, S.H., 2016. Systematic description of putative animal fossils from the Early Ediacaran Lantian Formation of South China. Palaeontology, 59, 515–532.
Wang, J., Li, Z.X., 2003. History of Neoproterozoic rift basins in South China: implications for Rodinia break-up. Precambrian Research, 122, 141–158.
Wang, J.S., Jiang, G.Q., Xiao, S.H., Li, Q., Wei, Q., 2008. Carbon isotope evidence for widespread methane seeps in the ca. 635 Ma Doushantuo cap carbonate in south China. Geology, 36, 347–350.
Wang, W., Zhou, C.M., Guang, C.G., Yuang, X.L., Chen, Z., Wan, B., 2014. An integrated carbon, oxygen, and strontium isotopic studies of the Lantian Formation in South China with implications for the Shuram anomaly. Chemical Geology, 373, 10–26.
Wang, W., Guan, C.G., Zhou, C., Peng, Y., Pratt, L.M., Chen, X., Chen, L., Chen, Z., Yuan, X., Xiao, S., 2017. Integrated carbon, sulfur, and nitrogen isotope chemostratigraphy of the Ediacaran Lantian Formation in South China: Spatial gradient, ocean redox oscillation, and fossil distribution. Geobiology, 15, 552–571.
Wang, X.Q., Jiang, G.Q., Shi, X.Y., Peng, Y.B., Morales, D., 2018. Nitrogen isotope constraints on the early Ediacaran ocean redox structure. Geochimica et Cosmochimica Acta, in press.
Xiao, S.H., Zhang, Y., Knoll, A.H., 1998. Three-dimensional preservation of algae and animal embryos in a Neoproterozoic phosphorite. Nature, 391, 553–558.
Xiao, S., Zhou, C., Yuan, X., 2007. Undressing and redressing Ediacaran embryos. Nature, 446, E10–E11.
Xiao, S.H., Zhou, C.M., Liu, P.J., Wang, D., Yuan, X.L., 2014. Phosphatized acanthomorphic acritarchs and related microfossils from the Ediacaran

Doushantuo Formation at Weng'an (South China) and their implications for biostratigraphic correlation. Journal of Paleontology, 88, 1–67.

Xiao, S.H., Narbonne, G.M., Zhou, C.M., Laflamme, M., Grazhdankin, D.V., Moczydlowska-Vidal, M., Cui, H., 2016. Towards an Ediacaran Time Scale: Problems, Protocols, and Prospects. Episodes 39, 540–555.

Yang, J.D., Sun, W.G., Wang, Z.Z., Xue, Y.S., Tao, X.C., 1999. Variations in Sr and C isotopes and Ce anomalies in successions from China: Evidence for the oxygenation of Neoproterozoic seawater? Precambrian Research, 93, 215–233.

Yin, L.M., Zhu, M.Y., Knoll, A.H., Yuan, X.L., Zhang, J.M., Hu, J., 2007. Doushantuo embryos preserved inside diapause egg cysts. Nature, 446, 661–663.

Zhang, S.H., Jiang, G.Q., Zhang, J.M., Song, B., Kennedy, M.J., Christie-Blick, N., 2005. U-Pb sensitive high-resolution ion microprobe ages from the Doushantuo Formation in south China: constraints on late Neoproterozoic glaciations. Geology, 33, 473–476.

Zhou, C.M., Xiao, S.H., 2007. Ediacaran $\delta^{13}C$ chemostratigraphy of South China. Chemical Geology, 237, 89–108.

Zhou, C.M., Guan, C.G., Cui, H., Ouyang, Q., Wang, W., 2016. Methane-derived authigenic carbonate from the lower Doushantuo Formation of South China: Implications for seawater sulfate concentration and global carbon cycle in the early Ediacaran ocean. Palaeogeography, Palaeoclimatology, Palaeoecology, 461, 145–155.

Zhou, C.M., Xiao, S.H., Wang, W., Guan, C.G., Ouyang, Q., Chen, Z., 2017. The stratigraphic complexity of the middle Ediacaran carbon isotopic record in the Yangtze Gorges area, South China, and its implications for the age and chemostratigraphic significance of the Shuram excursion. Precambrian Research, 288, 23–38.

Zhu, M.Y., Zhang, J.M., Steiner, M., Yang, A.H., Li, G.X., Erdtmann, B.D., 2003. Sinian-Cambrian stratigraphic framework for shallow- to deep-water environments of the Yangtze Platform: an integrated approach. Progress in Natural Science, 13, 951–960.

Zhu, M.Y., Zhang, J., Yang, A., 2007. Integrated Ediacaran (Sinian) chronostratigraphy of South China. Palaeogeography, Palaeoclimatology, Palaeoecology, 254, 7–61.

Zhu, M.Y., 2010. The origin and Cambrian explosion of animals: Fossil evidences from China. Acta Palaeontologica Sinica, 49, 269–287.

Zhu, M.Y., Lu, M., Zhang, J.M., Zhao, F.C., Li, G.X., Yang, A.H., Zhao, X., Zhao, M.J., 2013. Carbon isotope chemostratigraphy and sedimentary facies evolution of the Ediacaran Doushantuo Formation in western Hubei, South China. Precambrian Research, 225, 7–28.

Figure and table captions

Figure 1 (A) Geological map of China with the Yangtze platform highlighted in purple color. (B) Reconstructed Ediacaran depositional environments on the Yangtze platform (Jiang et al., 2011). Red star marks the location studied in this paper. (C) Sketch diagram showing sedimentary facies variations of the Doushantuo Formation within the middle Yangtze Platform (Zhu et al., 2013).

Figure 2 Shale from the upper Doushantuo Formation in the Wangjiapeng drill core (A, B). (A) Scanned image of polished thin section, sample number DST217, stratigraphic height 174.4 m. (B) BSE image of polished thin section, sample number DST217, stratigraphic height 174.4 m. Dolostone from the middle Doushantuo Formation in the Wangjiapeng drill core (C, D). (C) Scanned image of polished thin section, sample number DST115, stratigraphic height 94.2 m. (D) BSE image of polished thin section, sample number DST115, stratigraphic height 94.2 m.

Figure 3 Muddy dolostone from the lower Doushantuo Formation in the Wangjiapeng drill core. (A) Scanned image of polished thin section, sample number DST041, stratigraphic height 31.8 m. (B) BSE image of polished thin section, sample number DST041, stratigraphic height 31.8 m. (C) Scanned image of polished thin section, sample number DST089, stratigraphic height 73.4 m. Note this sample bears calcite veins. (D) BSE image of polished thin section, sample number DST089, stratigraphic height 73.4 m.

Figure 4 Organic-rich limestone from the lower Doushantuo Formation in the Wangjiapeng drill core. (A) Scanned image of polished thin section, sample number DST057, stratigraphic height 44.6 m. (B) BSE image of polished thin section, sample number DST057, stratigraphic height 44.6 m. (C) Scanned image of polished thin section, sample number DST069, stratigraphic height 54.2 m. Note this sample bears chert veins. (D) BSE image of polished thin section, sample number DST069, stratigraphic height 54.2 m.

Figure 5 Muddy limestone from the upper Doushantuo Formation in the Wangjiapeng drill core. (A) Scanned image of polished thin section, sample number DST193, stratigraphic height 156 m. (B) BSE image of polished thin section, sample number DST193, stratigraphic height 156 m.

Figure 6 Integrated time-series elemental and isotopic data from the Doushantuo Formation at the Wangjiapeng section. DST271 and DST311 are marked by different symbols as indicated by filled green color, because they might have suffered post-depositional alteration. Arrows indicate the decreasing trend of $\delta^{15}N$ values.

Figure 7 Cross plots of isotope and elemental data of the Doushantuo Formation at the Wangjiapeng section to help evaluate diagenetic effects.

Figure 8 Carbonate carbon isotope ($\delta^{13}C_{carb}$) and strontium isotope ($^{87}Sr/^{86}Sr$) chemostratigraphic correlations of the Ediacaran Doushantuo Formation across the Yangtze platform. Data of the Jiulongwan, Zhongling and Yangjiaping sections are from Cui et al. (2015) and the literature cited therein, whereas those of Wangjiapeng section are from this study.

Figure 9 Carbonate carbon isotope ($\delta^{13}C_{carb}$) and organic carbon isotope ($\delta^{13}C_{org}$) chemostratigraphic correlations of the Ediacaran Doushantuo Formation across the platform. Data of the Jiulongwan, Zhongling and Yangjiaping sections are from Cui et al. (2015) and literatures cited therein, whereas those of Wangjiapeng section are from this study.

Figure 10 Spatial variations in $\delta^{15}N$ values of the Doushantuo Formation and its stratigraphic equivalent Lantian Formation. Also indicated is the relative paleobathymetric location of sections on simplified cross section within the Yangtze Platform (Jiang et al., 2011). $\delta^{15}N$ values of the Yangtze Gorges section, Yangjiaping section and Lantian section are from Kikumoto et al. (2014), Ader et al. (2014) and Wang et al. (2017), respectively, whereas those of the Wangjiapeng section is from the current study.

Table 1 High-resolution geochemical data of the Doushantuo Formation at Wangjiapeng section.

Table 1 Isotopic and geochemical data

	Sample ID	Formation	Member	Depth (m)	Rock name	dissolve rate (%)	Sr (ppm)	Al (ppm)	Si (ppm)	K (ppm)	Mn (ppm)	Fe (ppm)	Mn/Sr	Rb/Sr	$\delta^{13}C_{car}$ (‰ vs.PDB)
0	DST001	Doushantuo	I	712.40	calcareous shale	45.52	192	127	294	15	934	418	4.867	0.0002	-3.45
1.6	DST003	Doushantuo	I	710.80	dolostone	89.87	243	506	426	23	1355	1285	5.588	0.0003	-3.11
2.4	DST005	Doushantuo	I	710.00	dolostone	91.35	127	562	527	52	718	1222	5.645	0.0011	-3.33
4.8	DST007	Doushantuo	I	707.58	calcareous shale	41.59	451	1258	485	458	636	2398	1.410	0.0014	3.23
6.4	DST009	Doushantuo	I	706.03	muddy dolostone	53.43	123	1072	488	327	1430	3456	11.619	0.0036	1.11
8.0	DST011	Doushantuo	I	704.43	siltstone	8.68	99	950	516	121	119	1031	1.206	0.0058	1.98
8.6	DST013	Doushantuo	I	703.79	siltstone	9.85	93	933	524	140	128	962	1.380	0.0065	2.49
11.8	DST017	Doushantuo	I	700.60	calcareous shale	49.52	264	944	550	130	656	1774	2.483	0.0027	3.96
13.4	DST019	Doushantuo	II	699.01	muddy dolostone	57.18	317	535	613	168	256	2043	0.809	0.0013	4.78
15.0	DST021	Doushantuo	II	697.43	muddy dolostone	58.27	292	345	562	113	207	2198	0.709	0.0011	5.20
16.6	DST023	Doushantuo	II	695.81	calcareous shale	49.64	281	599	671	251	168	1878	0.598	0.0019	5.52
18.2	DST025	Doushantuo	II	694.21	muddy dolostone	63.44	289	357	590	170	233	2719	0.805	0.0012	5.06
19.8	DST027	Doushantuo	II	692.58	muddy dolostone	61.37	331	443	679	223	266	2841	0.803	0.0012	5.07
21.4	DST029	Doushantuo	II	691.01	muddy dolostone	57.87	338	288	421	130	191	3078	0.564	0.0008	5.40
23.8	DST031	Doushantuo	II	688.61	muddy dolostone	56.97	307	327	502	239	172	3354	0.560	0.0014	5.50
25.4	DST033	Doushantuo	II	687.02	muddy dolostone	55.63	271	343	543	313	182	3376	0.670	0.0018	5.39
28.6	DST037	Doushantuo	II	683.83	muddy dolostone	52.89	219	224	418	264	141	4031	0.644	0.0017	5.30
30.2	DST039	Doushantuo	II	682.21	muddy dolostone	51.98	277	371	454	411	153	3589	0.552	0.0023	5.45
31.8	DST041	Doushantuo	II	680.63	muddy dolostone	54.58	330	716	651	772	161	3581	0.487	0.0029	5.69
33.4	DST043	Doushantuo	II	679.03	muddy dolostone	52.76	309	503	542	557	173	4259	0.561	0.0025	5.90
35.0	DST045	Doushantuo	II	677.43	dolostone	86.59	194	123	244	143	201	2712	1.036	0.0008	5.91
36.6	DST047	Doushantuo	II	675.81	muddy dolostone	56.26	377	347	626	359	194	6543	0.514	0.0013	6.40
38.2	DST049	Doushantuo	II	674.19	limestone	88.91	313	70	128	70	93	821	0.296	0.0003	6.56
39.8	DST051	Doushantuo	II	672.62	limestone	94.81	1007	99	151	59	45	912	0.044	0.0001	7.32
41.4	DST053	Doushantuo	II	671.02	limestone	90.31	965	84	149	83	53	931	0.055	0.0001	7.47
43.0	DST055	Doushantuo	II	669.41	limestone	95.77	1211	67	96	49	25	912	0.021	0.0001	7.88
44.6	DST057	Doushantuo	II	667.82	limestone	97.11	1257	33	63	22	21	872	0.017	0.0000	8.15
46.2	DST059	Doushantuo	II	666.21	limestone	85.73	1118	81	136	57	73	867	0.065	0.0001	7.52
47.8	DST061	Doushantuo	II	664.61	muddy limestone	73.30	790	109	217	77	58	846	0.073	0.0001	6.93
49.4	DST063	Doushantuo	II	663.02	limestone	75.80	1103	136	231	116	83	881	0.075	0.0002	7.45
51.0	DST065	Doushantuo	II	661.42	limestone	84.53	521	107	195	100	60	998	0.116	0.0002	6.98
52.6	DST067	Doushantuo	II	659.82	limestone	82.19	384	108	215	109	50	804	0.132	0.0004	7.96
54.2	DST069	Doushantuo	II	658.21	limestone	80.79	438	122	246	110	77	1486	0.175	0.0004	6.97
55.8	DST071	Doushantuo	II	656.63	limestone	80.92	412	182	323	182	77	1424	0.188	0.0005	6.64

57.4	DST073	Doushantuo	II	655.04	muddy limestone	59.49	316	312	513	351	153	3440	0.485	0.0013	7.46
59.0	DST075	Doushantuo	II	653.44	calcareous shale	49.83	298	403	956	432	132	4367	0.443	0.0019	7.98
65.4	DST079	Doushantuo	II	647.01	muddy limestone	51.74	452	470	576	402	151	3559	0.334	0.0017	6.75
67.0	DST081	Doushantuo	II	645.41	muddy limestone	52.60	405	371	740	420	179	5368	0.441	0.0014	6.69
68.6	DST083	Doushantuo	II	643.81	calcareous shale	27.92	206	577	598	691	87	3647	0.420	0.0047	6.24
70.2	DST085	Doushantuo	II	642.20	muddy dolostone	52.60	392	493	681	536	205	6354	0.523	0.0017	6.40
71.8	DST087	Doushantuo	II	640.61	muddy dolostone	50.66	334	572	446	645	183	5946	0.549	0.0024	6.75
73.4	DST089	Doushantuo	II	639.03	muddy dolostone	56.29	383	323	501	321	196	6783	0.512	0.0011	6.46
75.0	DST091	Doushantuo	II	637.42	muddy dolostone	58.01	401	385	1005	391	176	6054	0.439	0.0013	6.27
76.6	DST093	Doushantuo	II	635.81	calcareous shale	47.34	255	421	1172	475	149	5292	0.587	0.0025	6.11
78.2	DST095	Doushantuo	II	634.22	muddy dolostone	52.41	246	489	586	536	163	5607	0.661	0.0027	6.17
79.8	DST097	Doushantuo	II	632.61	muddy dolostone	58.19	388	535	583	519	139	6395	0.359	0.0020	6.90
81.4	DST099	Doushantuo	II	631.00	muddy dolostone	66.20	432	623	879	630	154	7072	0.356	0.0016	6.42
83.0	DST101	Doushantuo	II	629.41	muddy limestone	71.63	501	363	517	282	170	7650	0.340	0.0006	5.93
84.6	DST103	Doushantuo	II	627.81	muddy limestone	62.66	364	500	676	537	142	6483	0.391	0.0018	6.09
86.2	DST105	Doushantuo	II	626.23	muddy limestone	71.71	532	436	869	354	161	7708	0.303	0.0008	6.13
87.8	DST107	Doushantuo	II	624.61	muddy dolostone	55.09	324	470	995	562	118	5314	0.365	0.0026	5.98
89.4	DST109	Doushantuo	II	623.03	muddy dolostone	68.95	304	262	376	257	137	6088	0.450	0.0012	6.11
91.0	DST111	Doushantuo	II	621.41	dolostone	75.96	345	325	445	359	126	5012	0.366	0.0013	5.99
92.6	DST113	Doushantuo	II	619.83	dolostone	79.94	387	252	386	286	129	4937	0.333	0.0009	6.26
94.2	DST115	Doushantuo	II	618.22	dolostone	80.52	433	255	365	290	117	4631	0.270	0.0008	5.32
95.8	DST117	Doushantuo	II	616.59	muddy limestone	67.41	689	56	141	39	41	1447	0.060	0.0001	5.39
97.4	DST119	Doushantuo	II	615.02	limestone	91.21	372	53	119	55	37	1621	0.100	0.0003	6.51
98.9	DST121	Doushantuo	II	613.51	limestone	88.53	529	46	105	58	53	2030	0.099	0.0002	5.91
100.6	DST123	Doushantuo	II	611.82	muddy limestone	74.05	450	279	410	335	100	4118	0.222	0.0012	6.21
102.2	DST125	Doushantuo	II	610.23	muddy limestone	66.67	350	330	439	316	92	4178	0.264	0.0019	6.32
103.8	DST127	Doushantuo	II	608.61	muddy limestone	74.02	439	407	512	325	102	4518	0.233	0.0014	6.20
105.4	DST129	Doushantuo	II	607.01	muddy limestone	60.21	362	369	399	289	105	5047	0.291	0.0017	6.28
107.0	DST131	Doushantuo	II	605.43	muddy limestone	63.21	438	317	438	299	126	5666	0.287	0.0013	6.42
108.2	DST133	Doushantuo	II	604.23	limestone	94.73	353	49	107	57	125	1881	0.355	0.0003	2.90
109.8	DST135	Doushantuo	II	602.63	muddy limestone	72.76	520	56	189	70	58	1262	0.112	0.0002	5.07
111.4	DST137	Doushantuo	II	601.02	limestone	79.29	493	111	174	81	54	954	0.109	0.0005	5.87
113.6	DST139	Doushantuo	II	598.80	muddy limestone	71.47	486	149	285	109	75	1300	0.154	0.0006	6.05
115.3	DST141	Doushantuo	II	597.12	muddy limestone	74.89	426	192	272	178	68	1513	0.160	0.0016	6.21
117.2	DST143	Doushantuo	II	595.22	limestone	83.82	623	204	270	122	65	1387	0.104	0.0007	6.17
119.6	DST147	Doushantuo	II	592.81	muddy dolostone	57.65	929	752	909	408	141	2583	0.152	0.0015	5.95
120.8	DST149	Doushantuo	II	591.62	muddy dolostone	59.19	1019	527	755	340	146	2549	0.143	0.0011	5.99

122.4	DST151	Doushantuo	II	590.03	muddy dolostone	66.39	778	560	803	342	157	2953	0.201	0.0016	6.03
124.0	DST153	Doushantuo	II	588.41	calcareous shale	34.45	630	122	188	75	34	804	0.055	0.0004	5.57
125.6	DST155	Doushantuo	II	586.83	muddy limestone	59.10	669	122	468	184	57	983	0.085	0.0009	5.66
128.8	DST159	Doushantuo	II	583.62	calcareous shale	49.97	819	523	1349	761	68	1850	0.084	0.0028	5.74
130.4	DST161	Doushantuo	III	582.00	muddy limestone	52.63	810	438	1245	777	80	2294	0.099	0.0016	5.60
132.0	DST163	Doushantuo	III	580.42	muddy limestone	59.59	1118	490	1009	348	159	2422	0.142	0.0032	6.27
132.8	DST165	Doushantuo	III	579.62	muddy limestone	55.56	933	557	1347	558	142	2132	0.152	0.0025	6.27
136.0	DST167	Doushantuo	III	576.40	calcareous shale	39.53	723	610	1238	938	101	1667	0.140	0.0047	5.97
137.6	DST171	Doushantuo	III	574.83	calcareous shale	48.87	865	464	970	549	98	2829	0.113	0.0025	3.95
140.0	DST173	Doushantuo	III	572.41	muddy limestone	58.24	769	581	1177	675	103	2816	0.133	0.0032	4.03
141.6	DST175	Doushantuo	III	570.81	muddy dolostone	60.82	670	612	1194	512	173	2056	0.258	0.0035	6.61
144.8	DST179	Doushantuo	III	567.62	muddy dolostone	59.76	945	665	1408	473	227	2262	0.240	0.0027	6.04
146.4	DST181	Doushantuo	III	566.02	calcareous shale	45.38	777	539	1327	578	127	3307	0.163	0.0030	3.92
148.0	DST183	Doushantuo	III	564.41	calcareous shale	37.88	665	919	1432	819	107	2381	0.161	0.0044	4.10
149.6	DST185	Doushantuo	III	562.81	calcareous shale	47.64	598	613	1063	776	84	1383	0.140	0.0051	3.51
151.2	DST187	Doushantuo	III	561.22	muddy limestone	72.33	879	266	1481	353	75	1064	0.085	0.0016	4.59
154.4	DST191	Doushantuo	III	558.01	muddy limestone	69.01	876	375	1113	281	97	1460	0.111	0.0013	4.05
156.0	DST193	Doushantuo	III	556.41	muddy dolostone	61.88	743	665	1116	376	227	1367	0.306	0.0028	5.61
157.6	DST195	Doushantuo	III	554.81	muddy dolostone	50.54	665	655	1710	565	148	2239	0.223	0.0035	3.42
159.0	DST197	Doushantuo	III	553.42	muddy dolostone	52.01	830	709	2279	632	95	2285	0.115	0.0031	4.16
160.6	DST199	Doushantuo	III	551.82	calcareous shale	43.98	617	593	1763	773	99	1528	0.160	0.0047	4.46
162.2	DST201	Doushantuo	III	550.21	calcareous shale	49.47	608	352	839	602	126	2302	0.206	0.0036	4.02
163.8	DST203	Doushantuo	III	548.61	calcareous shale	33.10	1022	838	1240	937	85	1599	0.083	0.0033	2.59
165.3	DST205	Doushantuo	III	547.10	calcareous shale	49.07	600	609	1042	836	165	1765	0.275	0.0054	4.15
166.9	DST207	Doushantuo	III	545.50	calcareous shale	46.46	550	620	1039	646	137	2324	0.249	0.0048	3.72
168.4	DST209	Doushantuo	III	544.00	calcareous shale	49.38	696	819	1139	1154	147	3162	0.211	0.0062	3.04
170.0	DST211	Doushantuo	III	542.40	muddy dolostone	61.22	541	705	1220	447	221	1750	0.408	0.0038	3.72
171.2	DST213	Doushantuo	III	541.20	calcareous shale	36.12	612	880	999	1627	126	2204	0.206	0.0087	3.56
172.4	DST215	Doushantuo	III	540.00	calcareous shale	37.55	758	815	932	1615	169	3247	0.222	0.0079	3.26
174.4	DST217	Doushantuo	III	538.00	calcareous shale	45.49	717	739	1806	989	184	2031	0.256	0.0052	4.15
176.0	DST219	Doushantuo	III	536.40	calcareous shale	39.34	624	1088	2430	1193	173	1783	0.278	0.0069	3.87
177.7	DST221	Doushantuo	III	534.70	muddy dolostone	56.23	604	908	1276	458	217	1762	0.359	0.0040	2.71
179.2	DST223	Doushantuo	III	533.20	muddy dolostone	60.60	744	830	1525	257	191	2041	0.257	0.0017	2.93
180.8	DST225	Doushantuo	III	531.60	muddy dolostone	59.59	617	594	1543	610	183	2373	0.296	0.0033	0.27
182.4	DST227	Doushantuo	III	530.00	muddy dolostone	55.55	550	377	1729	449	103	1247	0.188	0.0028	4.35
183.8	DST229	Doushantuo	III	528.60	calcareous shale	34.60	484	823	1579	826	112	1438	0.231	0.0058	1.61
185.2	DST231	Doushantuo	III	527.20	muddy dolostone	60.30	481	691	1605	830	158	1402	0.329	0.0053	1.60

186.8	DST233	Doushantuo	III	525.60	muddy dolostone	53.75	543	497	1395	769	202	3235	0.372	0.0043	1.08
188.4	DST235	Doushantuo	III	524.00	muddy dolostone	50.89	429	481	1017	425	141	1611	0.329	0.0041	2.97
189.8	DST237	Doushantuo	III	522.60	calcareous shale	41.65	435	675	2518	754	129	1327	0.296	0.0057	2.86
191.4	DST239	Doushantuo	III	521.00	calcareous shale	26.46	363	800	790	812	67	1343	0.185	0.0067	2.77
193.0	DST241	Doushantuo	III	519.40	muddy dolostone	54.70	398	598	983	289	136	1345	0.341	0.0040	1.86
195.2	DST243	Doushantuo	III	517.20	muddy dolostone	52.67	475	511	581	282	108	1373	0.228	0.0029	2.97
196.4	DST245	Doushantuo	III	516.02	calcareous shale	45.19	404	486	538	572	105	1498	0.260	0.0043	3.34
198.0	DST247	Doushantuo	III	514.43	muddy dolostone	53.20	531	596	1825	760	189	1665	0.355	0.0049	2.82
199.6	DST249	Doushantuo	III	512.81	muddy dolostone	57.98	492	630	1264	279	127	1617	0.259	0.0034	2.10
202.7	DST253	Doushantuo	III	509.70	muddy dolostone	54.82	405	692	1925	881	173	1238	0.426	0.0068	-2.20
204.3	DST255	Doushantuo	III	508.10	muddy dolostone	57.08	380	615	1309	734	169	1434	0.445	0.0064	-1.21
205.9	DST257	Doushantuo	III	506.51	muddy dolostone	52.32	439	967	1662	1012	152	1159	0.346	0.0080	-2.27
207.5	DST259	Doushantuo	III	504.93	muddy dolostone	59.35	301	1039	1590	487	163	1304	0.543	0.0074	-1.36
209.1	DST261	Doushantuo	III	503.31	calcareous shale	34.25	377	1009	1765	928	98	1108	0.259	0.0090	-5.36
210.7	DST263	Doushantuo	III	501.72	calcareous shale	45.26	266	753	1296	913	165	1134	0.620	0.0106	-3.01
212.3	DST265	Doushantuo	III	500.12	muddy dolostone	53.54	237	818	2164	892	139	1205	0.584	0.0109	-1.89
213.9	DST267	Doushantuo	III	498.51	muddy dolostone	72.85	194	654	1259	209	216	1214	1.110	0.0056	3.75
215.3	DST269	Doushantuo	III	497.12	dolostone	77.24	153	495	998	205	162	1009	1.054	0.0053	3.37
216.9	DST271	Doushantuo	III	495.53	dolostone	81.05	246	478	1027	154	161	970	0.657	0.0029	0.47
220.5	DST275	Doushantuo	III	491.90	muddy dolostone	72.43	230	464	1282	575	133	795	0.580	0.0050	3.26
223.4	DST279	Doushantuo	III	489.02	limestone	77.41	212	90	1521	109	123	425	0.580	0.0015	3.73
225.0	DST281	Doushantuo	III	487.41	muddy dolostone	74.26	159	108	975	81	54	502	0.342	0.0013	6.35
226.6	DST283	Doushantuo	III	485.82	dolostone	84.36	233	80	572	97	65	747	0.278	0.0008	4.78
227.9	DST285	Doushantuo	III	484.51	dolostone	84.24	369	95	831	34	42	420	0.115	0.0003	5.41
229.5	DST287	Doushantuo	III	482.91	dolostone	88.17	158	73	1064	38	48	562	0.304	0.0006	5.44
232.7	DST291	Doushantuo	IV	479.72	dolostone	91.69	175	51	247	18	72	916	0.412	0.0003	3.02
234.3	DST293	Doushantuo	IV	478.14	dolostone	88.79	80	49	801	35	69	644	0.864	0.0011	3.39
235.9	DST295	Doushantuo	IV	476.53	dolostone	84.19	86	93	759	63	56	541	0.655	0.0018	3.77
239.1	DST299	Doushantuo	IV	473.31	dolostone	81.61	182	96	175	8	55	442	0.302	0.0000	1.66
253.9	DST311	Doushantuo	IV	458.50	dolostone	89.29	174	209	140	30	40	524	0.230	0.0002	4.26
255.4	DST313	Doushantuo	IV	457.00	dolostone	87.89	85	272	387	200	57	669	0.675	0.0025	5.43
257.2	DST315	Doushantuo	IV	455.20	dolostone	87.05	85	253	305	159	53	682	0.622	0.0020	5.65
246.4	DST317	Doushantuo	IV	466.00	dolostone	90.70	73	150	267	149	58	721	0.794	0.0019	2.81
247.7	DST319	Doushantuo	IV	464.70	dolostone	84.15	134	199	386	183	80	886	0.599	0.0015	3.51
249.2	DST321	Doushantuo	IV	463.20	dolostone	90.85	64	205	334	199	57	875	0.891	0.0028	2.85
250.7	DST323	Doushantuo	IV	461.70	dolostone	76.00	68	253	322	194	40	623	0.586	0.0039	4.93

$\delta^{13}C_{org}$ (‰ vs.PDB)	$\Delta^{13}C_{car-org}$ (‰ vs.PDB)	$\delta^{15}N_{TN}$ (‰ vs.AIR)	$\delta^{18}O_{car}$ (‰ vs.PDB)	$^{87}Sr/^{86}Sr$ measured	error (2σ)	Age (Ma)	$^{87}Sr/^{86}Sr$ initial
0	0	0.0	-10.90			> 551	
0	0	0.0	-11.29			> 551	
0	0	0.0	-6.29			> 551	
-20.9	24.18	4.9	-0.91	0.71186	0.00001	> 551	0.71182
-23.6	24.73	6.8	-3.12			> 551	
-27.7	29.72	7.7	-8.37			> 551	
-27.2	29.67	6.1	-7.41			> 551	
-26.7	30.64	7.3	-2.69			> 551	
-28.8	33.53	5.6	-5.99	0.70824	0.00002	> 551	0.70821
-28.8	34.04	6.7	-8.11			> 551	
-28.6	34.16	6.7	-7.52			> 551	
-27	32.06	5.7	-6.64			> 551	
-28.9	33.94	4.2	-5.88			> 551	
-28.9	34.27	5.0	-5.44	0.70828	0.00001	> 551	0.70826
-29	34.54	6.8	-4.66			> 551	
-29.1	34.46	6.7	-7.15			> 551	
-29.2	34.49	5.9	-8.01			> 551	
-29.2	34.64	5.8	-5.95			> 551	
0	0	0.0	-6.15			> 551	
-29.1	35	5.8	-5.23			> 551	
0	0	0.0	-8.98			> 551	
-28.9	35.26	6.5	-5.21	0.70811	0.00002	> 551	0.70808
0	0	0.0	-10.12			> 551	
0	0	0.0	-8.16	0.70823	0.00001	> 551	0.70823
0	0	0.0	-7.84			> 551	
0	0	0.0	-7.23	0.70801	0.00002	> 551	0.70801
0	0	0.0	-7.60	0.70830	0.00002	> 551	0.70830
0	0	0.0	-8.33	0.70871	0.00002	> 551	0.70871
-26.3	33.27	6.0	-7.65			> 551	
-29.3	36.77	3.1	-7.32	0.70804	0.00002	> 551	0.70804
-29	35.99	7.6	-8.61			> 551	
-29.4	37.4	6.0	-7.34			> 551	
-29.2	36.15	2.3	-8.31	0.70803	0.00002	> 551	0.70802
-28.6	35.27	2.9	-8.32			> 551	

-28.4	35.86	6.0	-5.14			>	551	
-28.6	36.57	5.2	-4.09			>	551	
-28.5	35.2	5.3	-4.66	0.70835	0.00001	>	551	0.70831
-28.7	35.37	4.2	-4.46			>	551	
-28.4	34.68	6.5	-5.24			>	551	
-28.1	34.45	5.3	-4.91			>	551	
-28.5	35.28	4.0	-4.43			>	551	
-28.3	34.8	2.9	-4.99			>	551	
-29	35.25	5.7	-4.82	0.70805	0.00002	>	551	0.70803
-29.3	35.41	5.3	-5.17			>	551	
-27.6	33.73	6.8	-5.35			>	551	
-28.5	35.43	5.2	-3.38			>	551	
-28.1	34.51	2.1	-4.24			>	551	
-28	33.88	4.7	-4.81	0.70811	0.00001	>	551	0.70809
-27.9	34.02	5.4	-4.34			>	551	
-27.9	34.04	6.6	-4.47	0.70809	0.00002	>	551	0.70807
-29	34.93	6.8	-4.18			>	551	
-30	36.07	4.3	-4.86	0.70816	0.00002	>	551	0.70814
-28.4	34.44	5.7	-4.88			>	551	
-28.8	35.11	5.8	-4.96			>	551	
-28.8	34.14	5.7	-5.86	0.70835	0.00002	>	551	0.70834
-29.1	34.47	7.6	-6.23	0.70813	0.00002	>	551	0.70813
0	0	0.0	-6.40			>	551	
-28.3	34.18	7.4	-6.67	0.70826	0.00002	>	551	0.70826
-29	35.2	5.0	-5.19			>	551	
-28.9	35.18	6.5	-5.50			>	551	
-28.9	35.08	6.1	-5.91	0.70807	0.00002	>	551	0.70804
-28.8	35.1	6.3	-4.58			>	551	
-28.9	35.31	1.3	-4.14			>	551	
0	0	0.0	-7.00			>	551	
-28.8	33.84	6.7	-7.01	0.70811	0.00002	>	551	0.70810
-27.9	33.8	8.2	-10.52	0.70887	0.00002	>	551	0.70886
-27.9	33.92	6.4	-9.32	0.70844	0.00002	>	551	0.70843
-28.4	34.65	7.1	-8.32			>	551	
-28.8	34.97	7.9	-9.19	0.70823	0.00002	>	551	0.70821
-28.7	34.67	6.8	-2.41			>	551	
-28.9	34.9	6.9	-1.88			>	551	

-28.8	34.85	7.5	-2.44			>	551	
-28.8	34.33	5.1	-8.13	0.70839	0.00002	>	551	0.70839
-27.9	33.58	7.6	-7.78			>	551	
-28.3	34.09	7.1	-5.26			>	551	
-28.5	34.09	8.1	-4.65	0.70820	0.00001	>	551	0.70817
-29	35.28	8.1	-2.99			>	551	
-29	35.3	7.5	-2.96			>	551	
-29	34.96	8.2	-3.06			>	551	
-28.5	32.42	7.8	-6.24			>	551	
-28.4	32.47	7.5	-7.72	0.70860	0.00002	>	551	0.70853
-28.8	35.44	8.3	-1.70			>	551	
-28.6	34.65	6.6	-1.82			>	551	
-28.3	32.23	8.4	-5.66			>	551	
-28.4	32.46	7.7	-4.80			>	551	
-28.6	32.15	8.3	-5.53			>	551	
-29.3	33.85	9.4	-7.36	0.70884	0.00001	>	551	0.70880
-28.7	32.77	6.3	-7.83	0.70888	0.00001	>	551	0.70885
-28.6	34.26	6.7	-1.60			>	551	
-28.4	31.79	6.5	-3.67			>	551	
-28.8	32.96	5.0	-5.48	0.70884	0.00002	>	551	0.70877
-29	33.49	6.0	-3.72			>	551	
-28.8	32.82	6.5	-4.45			>	551	
-28.8	31.42	4.7	-5.43			>	551	
-28.9	33.08	7.2	-2.05			>	551	
-29.2	32.88	6.2	-3.48			>	551	
-29.3	32.36	6.1	-4.05			>	551	
-28.7	32.42	4.2	-1.35	0.70845	0.00002	>	551	0.70837
-29.4	32.95	7.0	-3.47			>	551	
-29.4	32.64	6.3	-4.38			>	551	
-29.2	33.4	5.9	-2.44			>	551	
-28.7	32.58	7.1	-1.45			>	551	
-28.8	31.52	6.2	-1.00			>	551	
-28.8	31.69	4.8	-3.31	0.70877	0.00002	>	551	0.70873
-29.4	29.72	5.1	-5.12			>	551	
-29.7	34.06	6.1	-2.51			>	551	
-29.4	31.05	6.2	-3.12			>	551	
-29.2	30.82	5.9	-1.76			>	551	

-29.5	30.53	4.8	-4.42			>	551	
-29.4	32.36	7.1	-2.29	0.70853	0.00001	>	551	0.70844
-29.3	32.2	5.8	-2.22			>	551	
-30.6	33.39	5.8	-4.31			>	551	
-28.8	30.68	5.3	-1.73			>	551	
-30.4	33.39	7.0	-3.22	0.70852	0.00002	>	551	0.70846
-30.1	33.42	7.0	-3.03			>	551	
-29.2	31.98	7.2	-2.25			>	551	
-30.1	32.22	6.4	-3.02	0.70863	0.00002	>	551	0.70855
-28.9	26.7	5.6	-1.95			>	551	
-29.1	27.94	7.3	-2.48			>	551	
-28.2	25.97	7.0	-1.57			>	551	
-28.1	26.74	7.7	-1.74			>	551	
-28.8	23.45	7.0	-2.32			>	551	
-28.6	25.56	7.2	-2.21			>	551	
-28.8	26.95	5.3	-2.22			>	551	
-28.2	31.95	0.0	-1.77			>	551	
-28.6	32	0.0	-1.39			>	551	
-29.1	29.6	0.0	-5.94	0.70949	0.00001	>	551	0.70942
-29.7	32.92	6.7	-4.08			>	551	
-27.3	31.05	7.1	-5.07	0.70866	0.00002	>	551	0.70863
-28.3	34.68	6.6	-1.93			>	551	
-28.8	33.55	0.0	-4.26			>	551	
-28.9	34.27	0.0	-4.92	0.70874	0.00002	>	551	0.70873
-28.4	33.86	0.0	-4.12			>	551	
-28.8	31.79	0.0	-6.33			>	551	
-27.9	31.33	0.0	-6.40			>	551	
-27.7	31.46	0.0	-6.28			>	551	
-29.5	31.16	0.0	-6.75			>	551	
-29.8	34.04	3.5	-5.98	0.71308	0.00002	>	551	0.71307
-29.7	35.11	3.9	-4.14			>	551	
-29.3	34.97	3.7	-4.13			>	551	
-29.1	31.89	3.9	-4.11			>	551	
-29.9	33.46	4.0	-4.17	0.70840	0.00002	>	551	0.70836
-28.7	31.56	5.0	-3.77			>	551	
-30.3	35.22	4.2	-4.60	0.70990	0.00002	>	551	0.70982

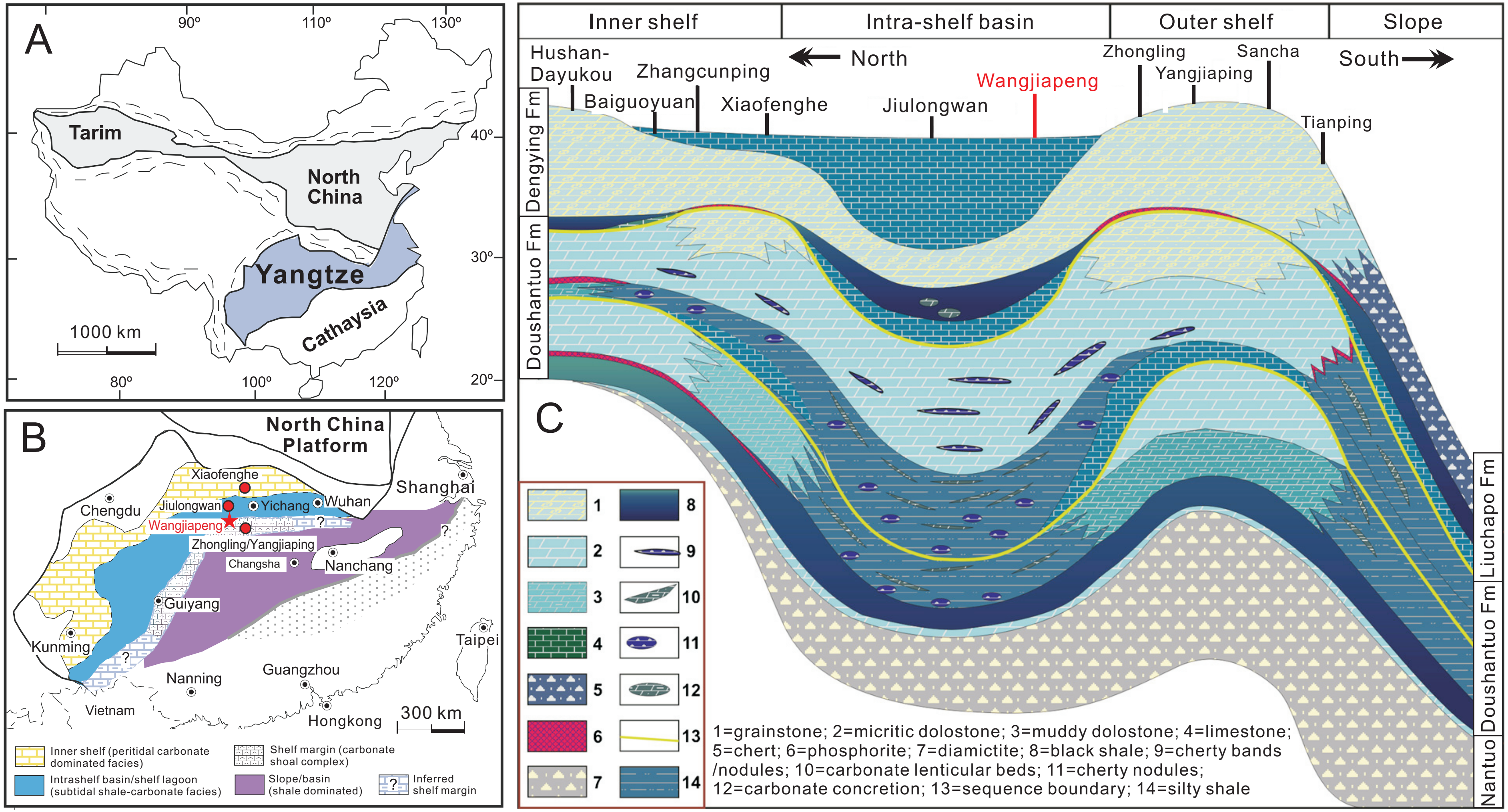

A
Tarim
North China
Yangtze
Cathaysia
1000 km
90°
110°
130°
40°
30°
20°
80°
100°
120°
B
North China Platform
Xiaofenghe
Chengdu
Jiulongwan
Yichang
Wuhan
Shanghai
Wangjiapeng
Zhongling/Yangjiaping
Changsha
Nanchang
Guiyang
Kunming
Taipei
Nanning
Guangzhou
Vietnam
Hongkong
300 km
Inner shelf (peritidal carbonate dominated facies)
Shelf margin (carbonate shoal complex)
Intrashelf basin/shelf lagoon (subtidal shale-carbonate facies)
Slope/basin (shale dominated)
Inferred shelf margin
C
Inner shelf
Intra-shelf basin
Outer shelf
Slope
North
South
Hushan-Dayukou
Baiguoyuan
Zhangcunping
Xiaofenghe
Jiulongwan
Wangjiapeng
Zhongling
Yangjiaping
Sancha
Tianping
Dengying Fm
Doushantuo Fm
Liuchapo Fm
Doushantuo Fm
Nantuo Fm
1=grainstone; 2=micritic dolostone; 3=muddy dolostone; 4=limestone; 5=chert; 6=phosphorite; 7=diamictite; 8=black shale; 9=cherty bands /nodules; 10=carbonate lenticular beds; 11=cherty nodules; 12=carbonate concretion; 13=sequence boundary; 14=silty shale

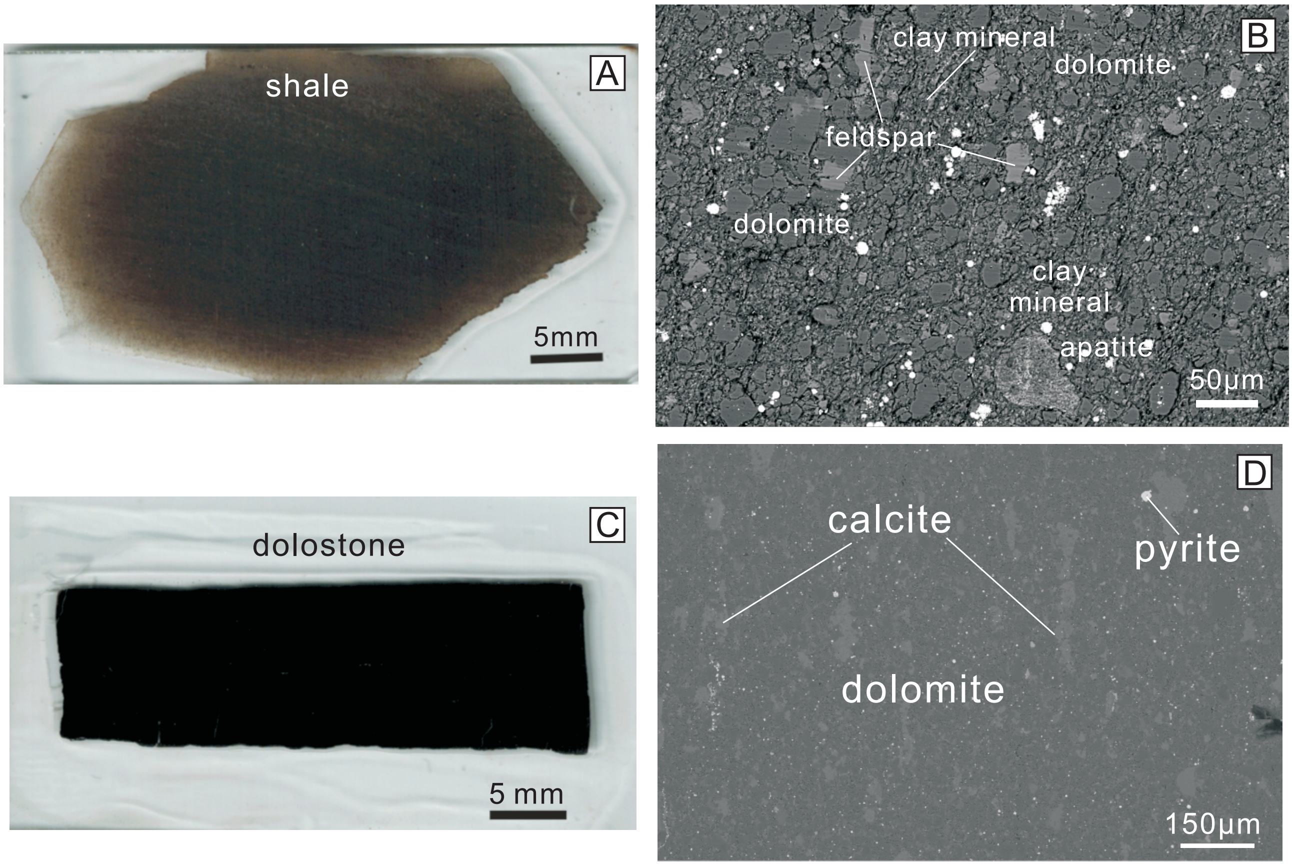
A
shale
5mm
B
clay mineral
dolomite
feldspar
dolomite
clay
mineral
apatite
50μm
C
dolostone
5 mm
D
calcite
pyrite
dolomite
150μm

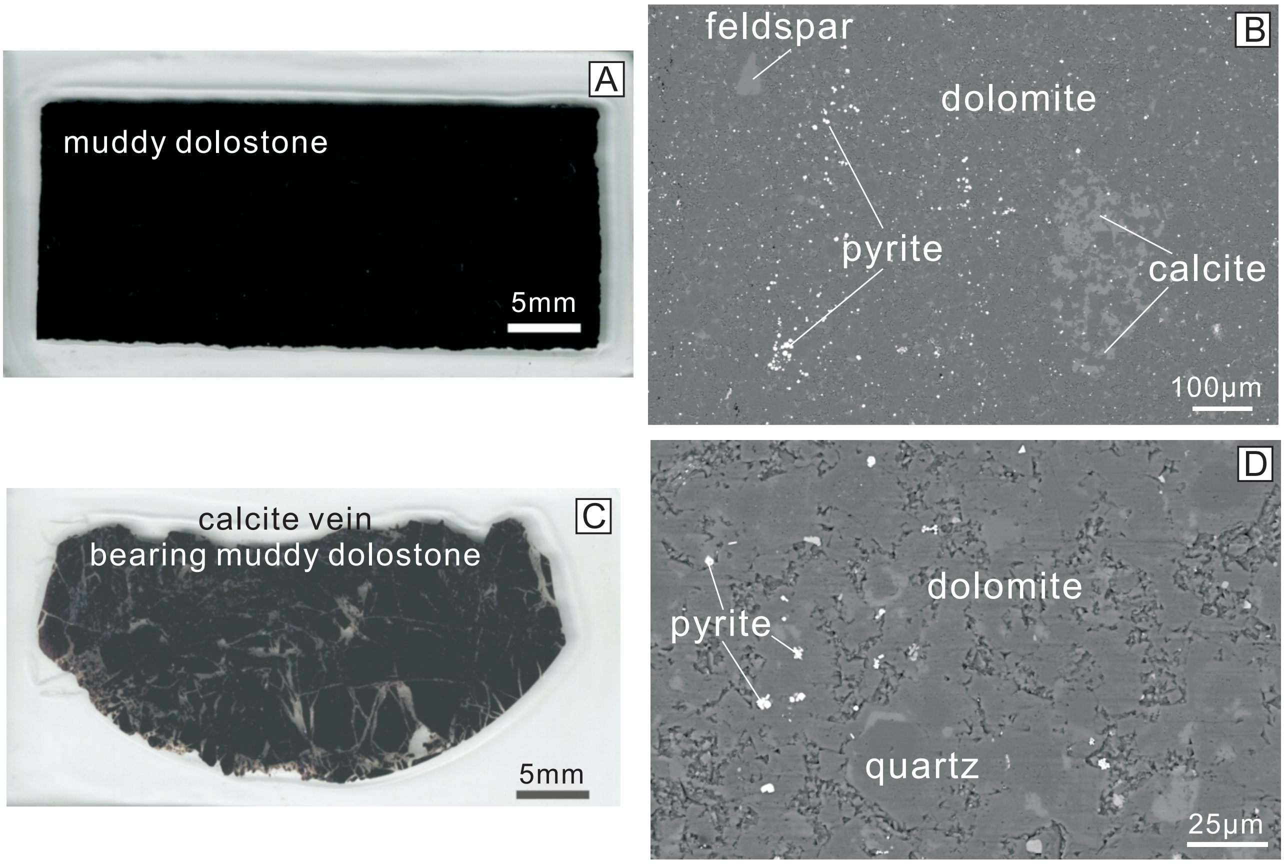
A
muddy dolostone
5mm
B
feldspar
dolomite
pyrite
calcite
100μm
C
calcite vein
bearing muddy dolostone
5mm
D
dolomite
pyrite
quartz
25μm

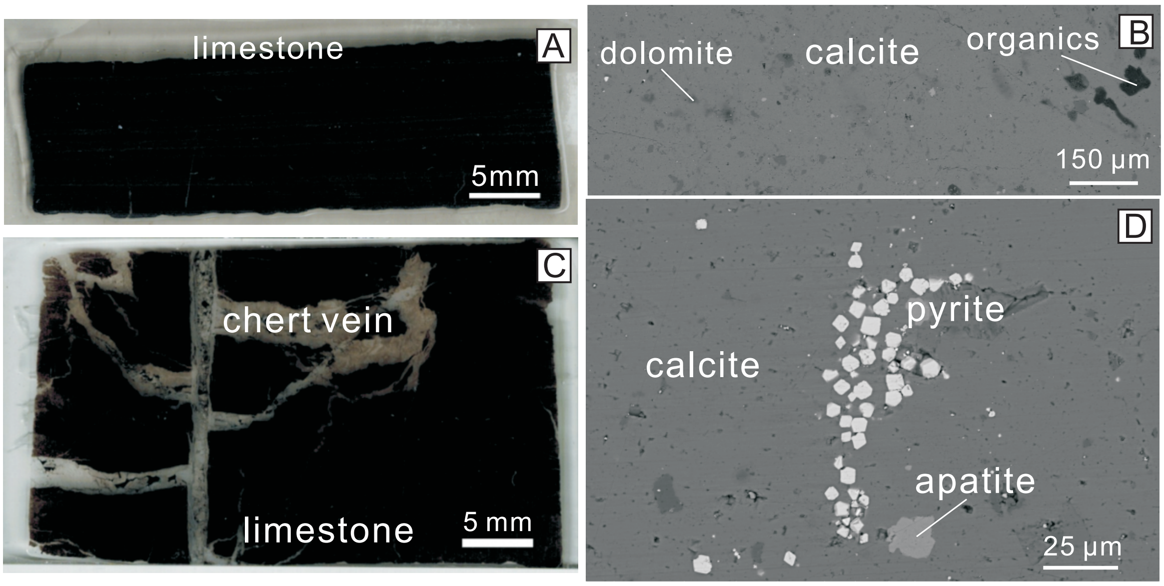
limestone
A
5mm
dolomite
calcite
organics
B
150 μm
chert vein
C
limestone
5 mm
D
pyrite
calcite
apatite
25 μm

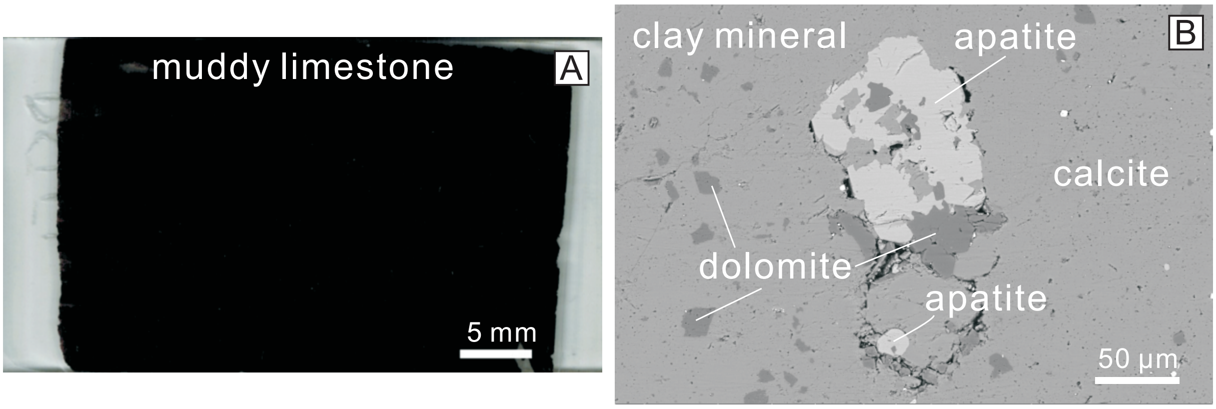
muddy limestone
A
5 mm
clay mineral
apatite
B
calcite
dolomite
apatite
50 μm

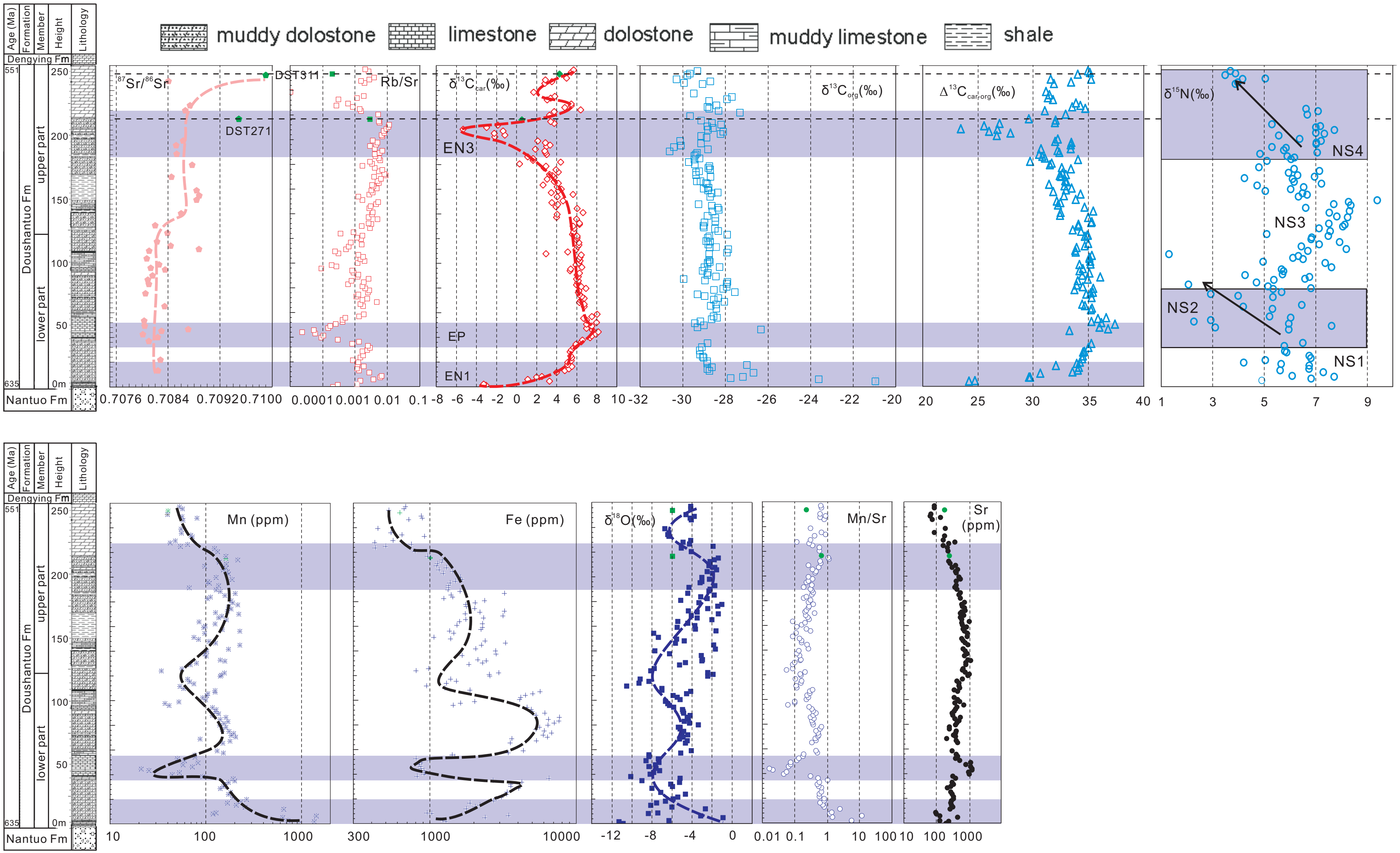

muddy dolostone
limestone
dolostone
muddy limestone
shale
Age (Ma)
Formation
Member
Height
Lithology
Dengying Fm
Doushantuo Fm
upper part
lower part
Nantuo Fm
551
635
250
200
150
100
50
0m
87Sr/86Sr
DST311
DST271
Rb/Sr
δ13Ccar(‰)
δ13Corg(‰)
Δ13Ccar-org(‰)
δ15N(‰)
EN3
EP
EN1
NS4
NS3
NS2
NS1
0.7076 0.7084 0.7092 0.7100
0.0001 0.001 0.01 0.1
-8 -6 -4 -2 0 2 4 6 8 10
-32 -30 -28 -26 -24 -22 -20
20 25 30 35 40
1 3 5 7 9
Mn (ppm)
Fe (ppm)
δ18O(‰)
Mn/Sr
Sr (ppm)
10 100 1000
300 1000 10000
-12 -8 -4 0
0.01 0.1 1 10 100
10 100 1000

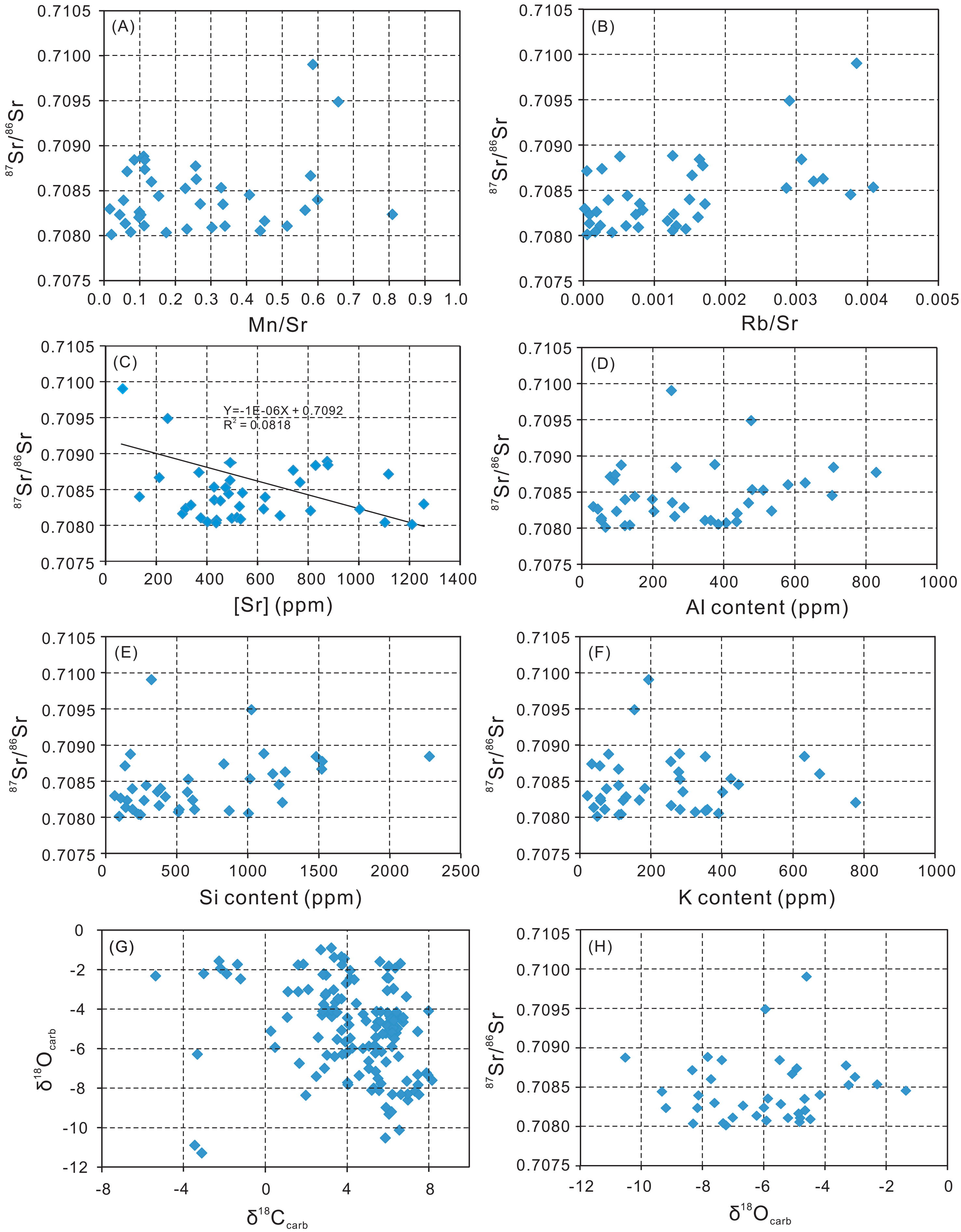
(A)
(B)
(C)
(D)
(E)
(F)
(G)
(H)
$^{87}Sr/^{86}Sr$
Mn/Sr
Rb/Sr
[Sr] (ppm)
Al content (ppm)
Si content (ppm)
K content (ppm)
Y=-1E-06X + 0.7092
R^2 = 0.0818
$\delta^{18}O_{carb}$
$\delta^{18}C_{carb}$

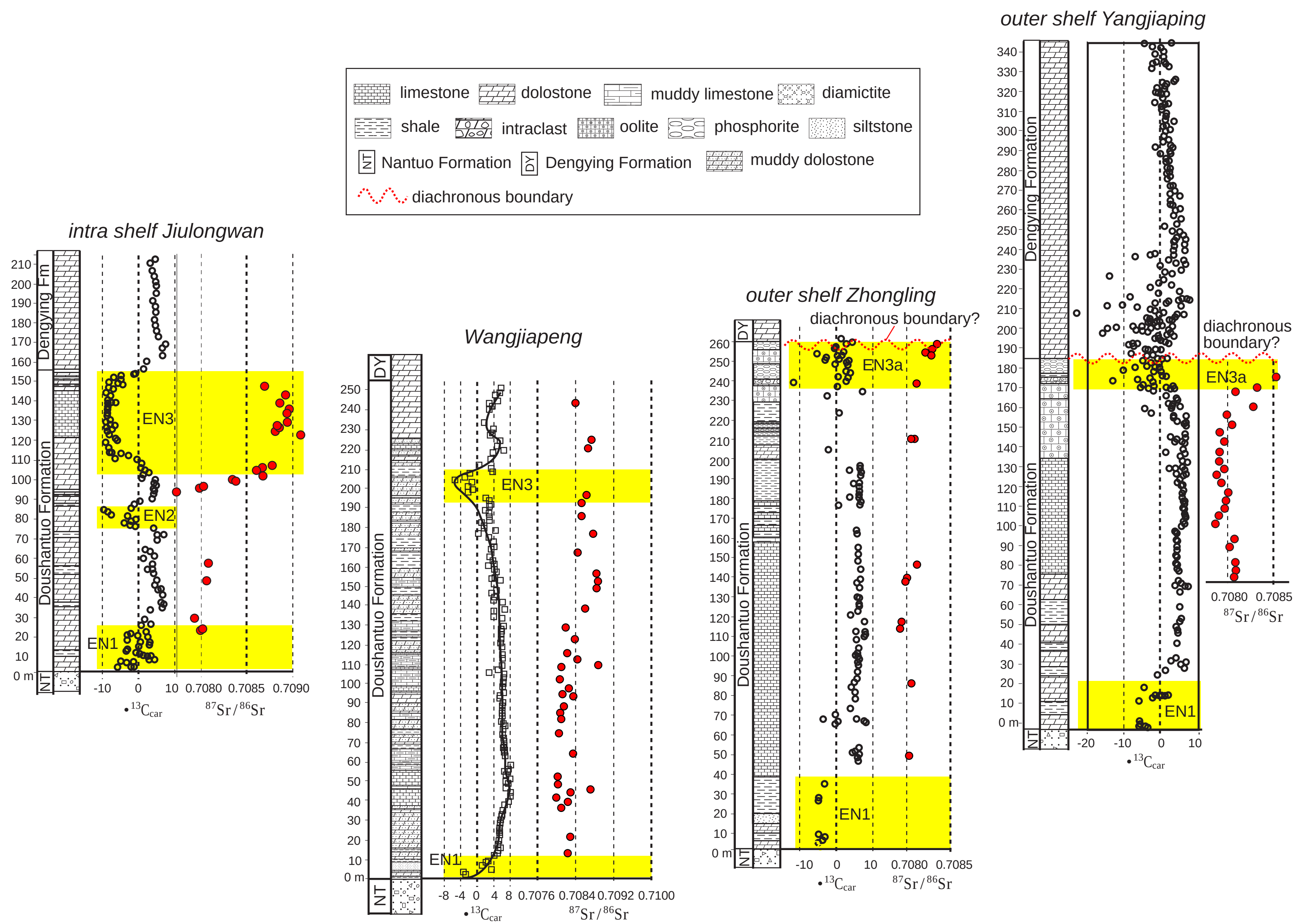

limestone
dolostone
muddy limestone
diamictite
shale
intraclast
oolite
phosphorite
siltstone
NT Nantuo Formation
DY Dengying Formation
muddy dolostone
diachronous boundary
intra shelf Jiulongwan
Wangjiapeng
outer shelf Zhongling
outer shelf Yangjiaping
Dengying Fm
Doushantuo Formation
Dengying Formation
EN1
EN2
EN3
EN3a
diachronous boundary?
$\delta^{13}C_{car}$
$^{87}Sr/^{86}Sr$

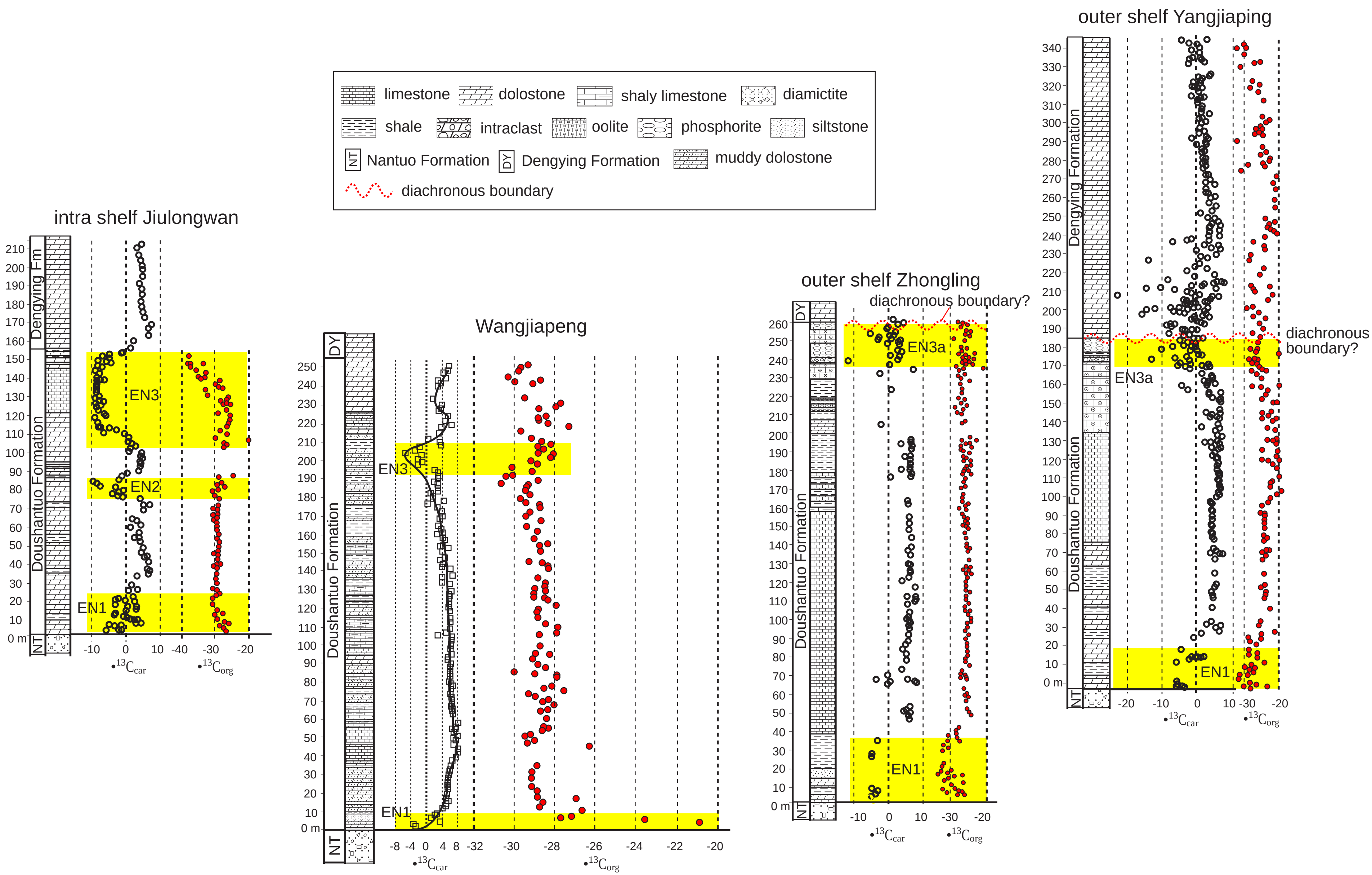

limestone
dolostone
shaly limestone
diamictite
shale
intraclast
oolite
phosphorite
siltstone
NT Nantuo Formation
DY Dengying Formation
muddy dolostone
diachronous boundary
intra shelf Jiulongwan
Dengying Fm
Doushantuo Formation
NT
EN1
EN2
EN3
13Ccar
13Corg
Wangjiapeng
DY
Doushantuo Formation
NT
EN1
EN3
13Ccar
13Corg
outer shelf Zhongling
diachronous boundary?
DY
Doushantuo Formation
NT
EN1
EN3a
13Ccar
13Corg
outer shelf Yangjiaping
Dengying Formation
Doushantuo Formation
NT
EN1
EN3a
diachronous boundary?
13Ccar
13Corg

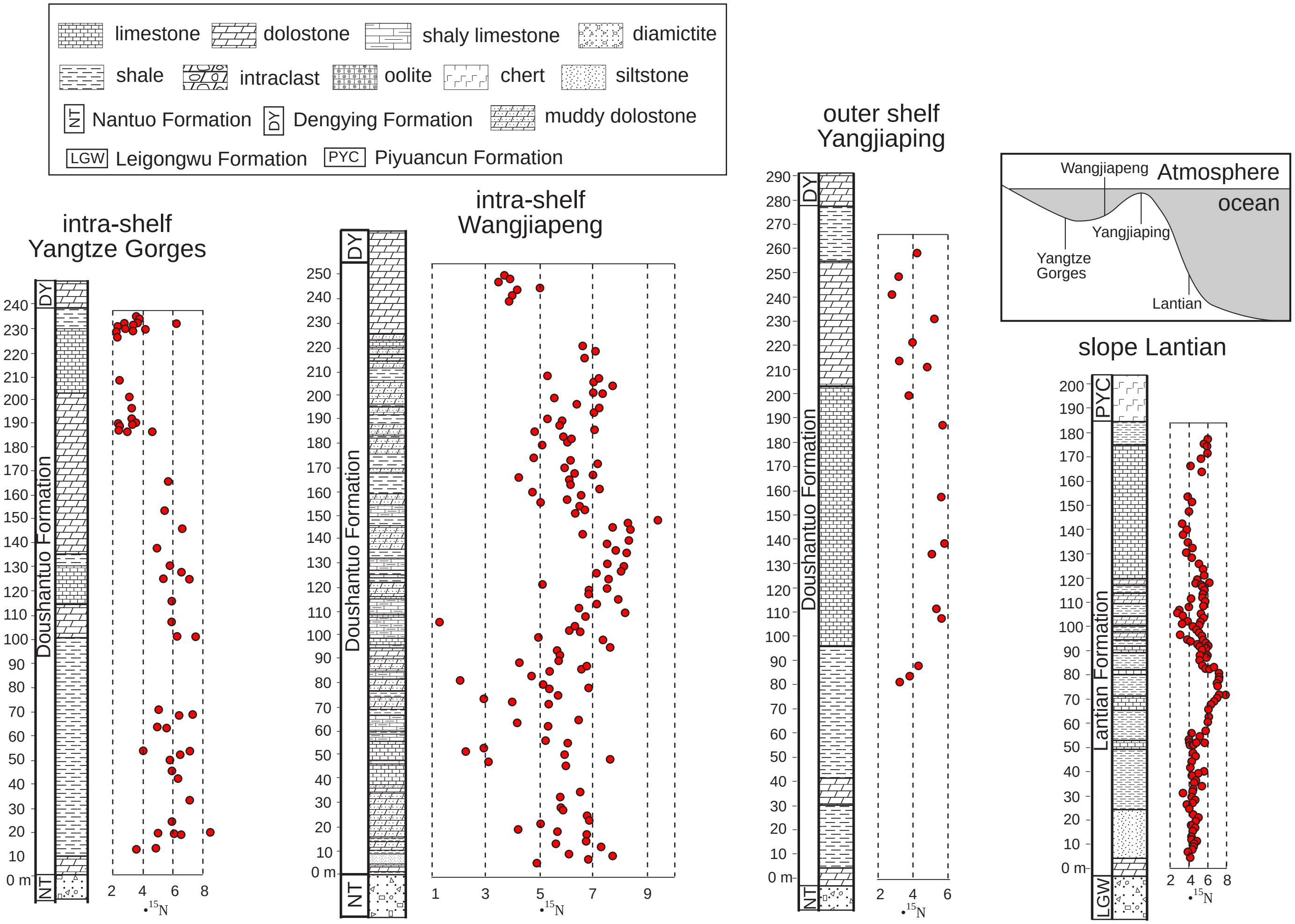

limestone
dolostone
shaly limestone
diamictite
shale
intraclast
oolite
chert
siltstone
NT Nantuo Formation
DY Dengying Formation
muddy dolostone
LGW Leigongwu Formation
PYC Piyuancun Formation
intra-shelf Yangtze Gorges
Doushantuo Formation
intra-shelf Wangjiapeng
outer shelf Yangjiaping
slope Lantian
Lantian Formation
Wangjiapeng
Atmosphere
ocean
Yangjiaping
Yangtze Gorges
Lantian